Decentralized PEV Power Allocation With Power Distribution and Transportation Constraints

Mushu Li, *Student Member, IEEE*, Jie Gao, *Member, IEEE*, Nan Chen,
Lian Zhao , *Senior Member, IEEE*, and Xuemin Shen, *Fellow, IEEE*

Abstract—**Plug-in Electric Vehicles (PEVs) keep on penetrating the automobile market. However, uncoordinated PEV charging can impair the reliability of power grid. In this paper, an interesting problem of PEV charging power allocation is investigated, in which both power distribution and transportation constraints are considered. A novel approach for PEV charging management based on optimal power flow (OPF) analysis is proposed to optimize PEV charging energy in a power distribution system. Firstly, spatial and temporal PEV demand scheduling is introduced to maximize PEV charging service capacity while considering the maximum traveling distance of PEVs. Secondly, to ensure the scalability of the OPF analysis, a distributed optimization technique, i.e., proximal Jacobian alternating direction multiplier method, is applied to attain the optimal power allocation in a decentralized manner. The resulting PEV charging service capacity in the power distribution system is improved without violating power distribution and transportation constraints. Furthermore, kernel density estimation method is adopted to identify the PEV range anxiety constraint without the PEV battery information. Simulation results are presented to validate the effectiveness of our approach with high PEV penetration.**

Index Terms—**Electric vehicles, charging management, range anxiety, distributed algorithm, alternating direction multiplier method (ADMM), kernel density estimation, smart grid.**

I. INTRODUCTION

RECENTLY, Plug-in Electric Vehicles (PEVs) have attracted public attention due to their low greenhouse gas emission, incentive legislation, and mature electric vehicle battery technologies [1]. The marketing stock of PEVs is expected to reach beyond 40 million by 2025 [2]. Nevertheless, high PEV penetration introduces the risk of degrading reliability and distribution efficiency in the power grid [3]. A large volume of PEV loads connected to the power distribution system increases the power transmission loss and voltage drop at distribution nodes [4]–[7]. Furthermore, the uncertainty

of PEV charging intensifies power profile fluctuation in a day, which also raises the likeliness of transformer overloading under the existing power grid infrastructure.

To mitigate the influence of PEV charging on the power grid, one direct approach is reinforcing the power grid infrastructure, which, however, requires significant capital expenditure and construction efforts. Alternatively, smart charging management is considered as an efficient method to improve PEV charging service capacity in the existing power grid [4]–[6]. Appropriate PEV charging power allocation schemes are applied to enable more PEVs charging simultaneously in the power grid without degrading its reliability. However, any charging management is constrained by the maximum traveling distance of PEVs and user tolerance on the charging delay, both of which add the difficulty on the management strategy design. Moreover, the algorithm complexity should not be neglected while measuring the effectiveness of a PEV charging management strategy. While conventional centralized PEV management is a common method to attain a globally optimal solution, it leads to high time-complexity due to large-scale system control [8]. In contrast, decentralized PEV charging management can decompose computation tasks to PEV charging stations (EVCSs), and each EVCS uses the local information to compute its local solution for PEV power allocation in a distributed manner. Consequently, compared with centralized PEV management, decentralized management can reduce time-complexity and enable parallel computing in PEV power allocation. However, it is challenging to achieve global optimality without complete knowledge of the whole power grid.

In literature, there are two main methods to increase service capacity for PEV charging: temporal demand scheduling [4], [7], [9]–[16] and spatial demand scheduling [16]–[18]. In the context of temporal demand scheduling, the main strategy of PEV management is extending or rescheduling the PEV charging process such that some power demand during peak hours can be shifted to fill the demand valley during non-peak hours. The works [9]–[11] propose temporal demand scheduling schemes to flatten the power profile during a day by directly controlling PEV charging process in an on-off charging method. However, PEV charging experience is not taken into consideration. The works [12]–[14] discuss indirect price control methods to manage the charging demand and thereby ensuring system reliability, where the charging cost is a tool to regulate PEV charging behaviors. However, temporal demand scheduling is not always feasible to be implemented,

especially for time-sensitive PEV users in fast charging stations. In addition, spatial management explores the mobility nature of PEVs to increase the flexibility of charging demand scheduling. In this case, finding optimal EVCSs for PEVs is the primary objective since EVCS is the main recharging infrastructure, especially for high-density urban areas [19]. By assigning EVCSs to PEVs, power congestion and voltage drop in the distribution system can be relieved, while the range anxiety of PEVs and traveling costs become main challenges. The work [20] estimates PEV traveling range using a machine learning technique. The proposed algorithm analyzes the range anxiety of PEVs from the knowledge of their historical trips. The works [18], [21] propose the distributed charging station selection solution considering the range anxiety of PEVs. The work [16] formulates temporal-spatial scheduling problem for PEV charging into a mixed-integer linear programming problem. The proposed centralized management strategy balances factors including the reliability of the considered power distribution system, the communication delay, and PEV range anxiety. However, few studies have formulated PEV power allocation problem with optimal power flow analysis in a decentralized manner [19].

The objective of this paper is to maximize the overall energy allocated for PEV charging without overloading the power distribution system while considering the cost of the PEV charging management. PEV charging demand is scheduled by the proposed power allocation approach in both spatial and temporal dimensions. The contributions of this paper are summarized as follows:

1) A PEV charging management approach is proposed to allocate PEV charging power by solving a power flow optimization problem and guarantee power distribution reliability under high PEV penetration. The charging service capacity of the power distribution system is maximized by managing the charging demand in both temporal and spatial dimensions. Moreover, to address the issue of range anxiety, the proposed approach considers power distribution and transportation constraints. PEVs can only be spatially scheduled within their maximum traveling distance.

2) In PEV charging power allocation, we perform a decentralized optimal power flow (OPF) analysis to obtain an optimal PEV power allocation policy. A distributed optimization technique, i.e., proximal Jacobian alternating direction multiplier method (PJADMM), decomposes the global power flow optimization problem into multiple subproblems, thereby distributing the computation load into distribution nodes. Each node attains the optimal power flow with limited local parameter exchange among EVCSs.

3) For the scenario in which the PEV information for the offline optimization period is limited, we identify the range anxiety constraint in PEV spatial scheduling from historical PEV charging profile by kernel density estimation method. Extensive simulations, developed in VISSIM [22], are presented to validate the effectiveness of our proposed approach in a realistic suburban scenario.
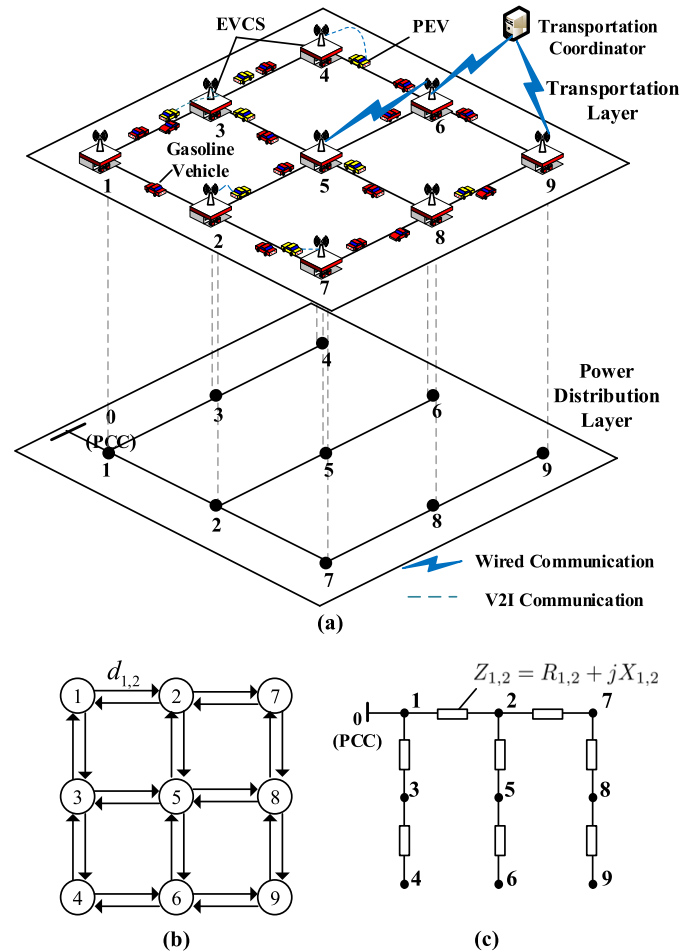

Fig. 1. (a) The system model of the PEV charging management network. (b) A 10-node sub-grid power distribution system. (c) The transportation network topology.

The remainder of the paper is organized as follows. The system model of the proposed work is given in Section II. The problem of PEV management is formulated in Section III. The optimal PEV power allocation scheme is developed in Section IV. The PEV charging parameter estimation method is discussed in Section V. Simulation results are provided in Sections VI, followed by concluding remarks in Section VII.

II. SYSTEM MODEL

The system model of a PEV charging management network is shown in Fig. 1(a). There are three layers in the proposed model: the power distribution layer, the transportation layer, and the communication layer. Section II-B and II-C will focus on introducing the power distribution layer and transportation layer, respectively. For the communication layer, each EVCS has an on-site roadside unit for exchanging the charging information with PEVs on the road through Vehicle-to-Infrastructure (V2I) communications [16]. The information exchange between a EVCS and its on-site roadside unit can be supported by IEC 61850 standard [23], [24]. A traffic coordinator monitors the number of PEV charging requests at all EVCSs and coordinates the spatial shifting of PEV units among EVCSs through wired communication links with EVCSs. EVCSs can also communicate with each other

Symbol	Definition	Symbol	Definition
e	index of PEV	$\bar{T}$	expected PEV parking time in an EVCS
h,k	index of bus/EVCS	T_c	number of slots for charging a PEV without interruption
l	distance	$v_{h,t}$	complex line-to-ground voltage at node h in slot t
t	index of time slot	$\mathbf{V}(t)$	voltage magnitude matrix in slot t
$\hat{t}$	time instant	$y_{h,k,t}$	number of PEV requesters to be shifted from h to k in slot t
B_e	battery capacity of PEV e		
C_{tem}	temporal PEV power shifting cost	$\bar{y}_{h,k}$	admittance between nodes h and k
$d_{h,k}$	length of the link (h,k)	$\mathbf{Y}$	admittance matrix
D_e	maximum traveling distance of PEV requester e	$\bar{z}_{h,k}$	impedance between adjacent nodes h and k
$E_{h,t}$	charging demand to be allocated at EVCS h in slot t	α, β	factors for the cost of spatial and temporal shifting
		$\gamma_{h,k,t}$	average number of PEV requesters that can be shifted from h to k in slot t
$\bar{E}_{h,t}$	charging demand that must be satisfied at EVCS h in slot t		
		$\Delta_{h,t}$	PEV power difference at EVCS h in slot t
F_e	maximum detouring range for charging of PEV e	$\lambda_{h,t}$	average PEV arrival rate at EVCS h in slot t
		ϖ	time length of a slot
$H_{h,t}$	power allocated for PEV loads at EVCS h in slot t	σ_t, σ_l	bandwidth of the Gaussian kernel
$i_{h,t}$	current injected into node h in slot t	$\mathcal{C}_h^G$	set of nodes connected to h directly in the grid topology
P_c	maximum charging power of a charger	$\mathcal{C}_h^T$	set of EVCSs connected to h directly in the transportation network
$p_{h,k,t}$	probability for PEV spatial shifting between node h and k in slot t		
		$\mathcal{E}$	set of edges in the transportation network
p_e^{con}	battery consumption rate	$\mathcal{G}$	set of EVCSs/buses
$P_{h,t}$	active power excluding PEV load at node h in slot t	$\mathcal{I}$	set of PEV requesters which arrived in the past
$\overline{P}_{h,t}$	active power upper bound at node h in slot t	$\mathcal{R}_{h,k,t}$	set of PEV requesters that can be shift to an EVCS k
$Q_{h,t}$	reactive power excluding PEV load at node h in slot t	$\mathcal{T}$	set of time slots
s_e	historical charging profile of PEV requesters e	$\mathcal{V}_{h,t}$	set of PEV requesters local to EVCS h in slot t
$S_{0,t}$	upper bound of the apparent power from PCC in slot t		

to exchange information for PEV power allocation through wired communication links. The summary of notations is given in Table I.

A. PEV Charging and EVCS Model

There are two types of vehicles on the road: PEVs and gasoline vehicles. Before a PEV with charging demand entering an EVCS, the PEV sends a charging request to the nearest EVCS. Denote the set of EVCSs as $\mathcal{G}$. PEVs which send charging request on the road are referred to as PEV requesters, and the EVCS receiving the request from PEV e is referred to as the "local" EVCS of PEV e in the remainder of the paper. Let $\mathcal{V}_{h,t}$ denote the set of PEV requesters local to EVCS h in time slot t, and $\mathcal{V}_{h,t} \cap \mathcal{V}_{k,t} = \emptyset$, for $\forall h, k \in \mathcal{G}$ and $h \neq k$. Each request contains the PEV's charging information, including its current state of charge, *i.e.*, SoC_e, the minimum required state of charge, *i.e.*, SoC_e^{min}, the battery capacity B_e, and the maximum detouring range for charging F_e. The current state of charge of PEV, *i.e.*, SoC_e, follows $\mathrm{SoC}_e \in [\mathrm{SoC}_e^{min}, 1]$. The distance between a PEV requester and its local EVCS is assumed to be under the maximum traveling range of PEVs.

The transportation coordinator collects the PEV requesters' information and provides the spatial shifting plan among EVCSs according to the power allocation result. Some PEV requesters can be scheduled to be charged at another EVCS within their maximum detouring range for charging, *i.e.*, F_e, and their maximum traveling range based on the remaining battery energy.

Once PEV e is plugged into an EVCS, due to the limited service capacity of the power distribution system, the charging process may be extended or interrupted to avoid the demand peak [25]. Temporal scheduling is applied in this step to allocate the charging power across time slots. Let E_{obj} be the objective PEV charging energy. For simplicity, we assume that E_{obj} is identical for all PEV requesters. The minimum number of time slots for fully charging a PEV without interruption can be calculated by EVCSs, which is denoted by T_c. It holds that $T_c = \lceil E_{obj}/(P_c \varpi) \rceil$, where P_c represents the maximum charging power, and ϖ represents the time length of a time slot. The expected PEV parking time in a charging station is denoted by $\bar{T}$, where $\bar{T} \geq T_c$. Temporal scheduling flexibility exists if $\bar{T} > T_c$. A PEV should be fully charged within $\bar{T}$ time slots after it is plugged into an EVCS.

B. Power Grid Model

The 10-node sub-grid power distribution network is presented in Fig. 1(c), where node 0 is the point of common coupling (PCC), and nodes 1 to 9 connect to power loads. There is one EVCS connected to each node except node 0. To simplify notations, an element of $\mathcal{G}$ represents either a node or an EVCS located at that node. Let $\bar{z}_{h,k}$ be the impedance between adjacent nodes h and k. We assume that power loads in each phase are balanced in the three-phase system having a tree structure [11], [26]. Thus, there is no loop in the topology of the power grid, and the single-phase power flow is analyzed.

We assume that the power demand for any time slot in the analysis time window $\mathcal{T}$ can be predicted [9]–[11], [16]. For each node, there are two types of power loads connecting to the grid: the PEV load at EVCSs, which will be managed by the

proposed charging strategy, and other power loads excluding the PEV load. For the PEV load, all PEVs connect to the power grid by DC connectors. Accordingly, only active power is allocated for the PEV load, which is a variable denoted as $H_{h,t}$ for $h \in \mathcal{G}$ at $t \in \mathcal{T}$. For other loads, the active and reactive power excluding PEV load at node h in time slot t are denoted by $P_{h,t}$ and $Q_{h,t}$, respectively. The grid has to satisfy power demand on $P_{h,t}$ and $Q_{h,t}$ and considers those demand as parameters in the power allocation. At each node except node 0, the overall active power from loads connected to node h cannot be greater than active power upper bound $\bar{P}_{h,t}$, i.e., $P_{h,t} + H_{h,t} \leq \bar{P}_{h,t}$, assuming $P_{h,t} \leq \bar{P}_{h,t}$. For node 0, we denote the active and reactive power drawing from PCC in time slot t as $P_{0,t}$ and $Q_{0,t}$, respectively. The term $\bar{S}_{0,t}$ denotes the upper bound of the apparent power draw from PCC in time t. Thus, it holds that $P_{0,t}^2 + Q_{0,t}^2 \leq \bar{S}_{0,t}^2, \forall t$.

Let $v_{h,t}$ and $i_{h,t}$ denote the complex line-to-ground voltage and the current injected into node $h \in \mathcal{G} \cup \{0\}$ at the t-th time slot, respectively. A voltage drop constraint restricts the voltage magnitude at each node: with the increasing load injection, the voltage magnitude for all nodes cannot be less than v_{min}. At node h, the relations between apparent power, voltage, and current are represented as following non-linear equations:

$$\begin{cases} v_{h,t} i_{h,t}^* = P_{h,t} + H_{h,t} + iQ_{h,t} & \text{, if } h \in \mathcal{G}, \\ v_{h,t} i_{h,t}^* = P_{0,t} + iQ_{0,t} & \text{, if } h = 0. \end{cases} \quad (1)$$

Furthermore, from Ohm's law, we have $\mathbf{i}(t) = \bar{\mathbf{Y}}\mathbf{v}(t)$, where $\mathbf{i}(t) = [i_{0,t}, \ldots, i_{|\mathcal{G}|,t}]^T$ and $\mathbf{v}(t) = [v_{0,t}, \ldots, v_{|\mathcal{G}|,t}]^T$. The symmetric admittance matrix $\bar{\mathbf{Y}}$ is defined as:

$$\begin{cases} \bar{y}_{h,h} = -\sum_{k \in \mathcal{C}_h^G} \bar{z}_{h,k}^{-1}, \\ \bar{y}_{h,k} = \bar{y}_{k,h} = \bar{z}_{h,k}^{-1}, & \forall k \in \mathcal{C}_h^G, \\ \bar{y}_{h,k} = \bar{y}_{k,h} = 0, & \forall k \notin \mathcal{C}_h^G \cup h, \end{cases} \quad (2)$$

where $\mathcal{C}_h^G$ represents the set of nodes which connect to node h directly in the grid topology. The term $\bar{y}_{h,k}$ represents the admittance between nodes h and k, which composes admittance matrix $\bar{\mathbf{Y}}$. For the tractability of considered relations, we rewrite equations in (1) in a linear model as in [26], [27]. Firstly, we define the admittance matrix only related to node h as:

$$\bar{\mathbf{Y}}_h = \mathbf{1}_h (\mathbf{1}_h)^T \bar{\mathbf{Y}}, \quad (3)$$

where $\mathbf{1}_h$ represents the vector in which only the h-th element is 1, and all other elements are 0. Furthermore, we define the voltage magnitude matrix in time slot t, $\mathbf{V}(t)$, as the outer-product matrix of voltage $\mathbf{v}(t)$, where $\mathbf{V}(t) = \mathbf{v}(t)\mathbf{v}(t)^H$. Thus, the diagonal elements of $\mathbf{V}(t)$ are the square of voltage magnitude for all nodes. After applying Ohm's Law, there exists a linear relation between the voltage magnitude matrix $\mathbf{V}(t)$ and power as shown in following equations:

$$\text{Tr}(\mathbf{1}_h(\mathbf{1}_h)^T \mathbf{V}(t)) = |v_{h,t}|^2 \quad (4a)$$
$$Re(\text{Tr}(\bar{\mathbf{Y}}_h \mathbf{V}(t))) = P_{h,t} + H_{h,t} \quad (4b)$$
$$Im(\text{Tr}(\bar{\mathbf{Y}}_h \mathbf{V}(t))) = Q_{h,t} \quad (4c)$$

As proved in [26], we reformulate Eqs. (4b) and (4c) in the form of hermitian matrices:

$$\text{Tr}(\mathbf{\Psi}_{P,h}\mathbf{V}(t)) = P_{h,t} + H_{h,t}; \quad \text{Tr}(\mathbf{\Psi}_{Q,h}\mathbf{V}(t)) = Q_{h,t}, \quad (5)$$

where hermitian matrices $\mathbf{\Psi}_{P,h}$ and $\mathbf{\Psi}_{Q,h}$ are defined as:

$$\mathbf{\Psi}_{P,h} = \frac{1}{2}(\bar{\mathbf{Y}}_h + (\bar{\mathbf{Y}}_h)^H); \quad \mathbf{\Psi}_{Q,h} = \frac{i}{2}(\bar{\mathbf{Y}}_h - (\bar{\mathbf{Y}}_h)^H). \quad (6)$$

Equation (5) establishes a linear relationship between PEV power $H_{h,t}$ and the voltage magnitude matrix $\mathbf{V}(t)$.

C. Transportation Graphic Model

Let a directed graph $\mathcal{G}_{TN} = (\mathcal{G}, \mathcal{E})$ represent the transportation network, as shown in Fig. 1(b), where $\mathcal{G}$ denotes the set of charging stations, and $\mathcal{E}$ denotes the set of edges. The directed link (h, k) represents the path from node h to node k. The term $d_{h,k}$ represents the length of the link (h, k). In the considered spatial scheduling, some PEV requesters local to EVCS h may be scheduled to be charged at another EVCS. Denote the number of PEV requesters to be shifted along the link (h, k) in time slot t as $y_{h,k,t}$.

When the distance among EVCSs cannot be negligible, the range anxiety constraints should be highlighted, which is referred to as the *range anxiety (RA)* scenario. Firstly, in the *RA* scenario, the length of all links in set $\mathcal{E}$ is under a distance threshold, θ_{max}, defined by the transportation coordinator. The threshold represents the maximum distance between two charging stations which can shift their PEV requesters to each other. If the distance between two EVCSs is longer than the threshold, no PEV requester will be shifted between the two EVCSs, and the corresponding link is not included in set $\mathcal{E}$. For EVCS h, set $\mathcal{C}_h^T$ represents the set of EVCSs connected directly to h in graph $\mathcal{G}_{TN}$, i.e., $d_{h,k} \leq \theta_{max}, \forall k \in \mathcal{C}_h^T$. In addition, PEV requesters can be shifted to another EVCS only if the distance to the EVCS is under their maximum traveling range. The spatial shifting for PEV requester e is constrained by two factors: the maximum detouring range for charging determined by the PEV's user, i.e., F_e, and the traveling range according to the remaining battery capacity. The maximum traveling range for PEV e can be formulated as the following equation:

$$D_e = \min\{F_e, [(\text{SoC}_e - \text{SoC}_e^{\min})B_e]/(p_e^{\text{con}})\}, \quad (7)$$

where D_e denotes the maximum traveling distance of PEV requester e. The parameter p_e^{con} represents the battery consumption rate with the unit of kWh/km. The parameter F_e depends on the willingness of the PEV driver for spatial shifting. When PEVs request to be charged at a charging station on the half of their route, their F_e will be relatively high. Otherwise, when PEVs consider the local charging station as their destination, they may set a low F_e to avoid spatial shifting. In EVCS h, the set of PEV requesters that can be shift to an EVCS $k \in \mathcal{C}_h^T$ is denoted by set $\mathcal{R}_{h,k,t}$, where $\mathcal{R}_{h,k,t} \subseteq \mathcal{V}_{h,t}$. The maximum traveling range of all PEVs in $\mathcal{R}_{h,k,t}$ should be over the link length between EVCS h and k, i.e., $D_e \geq d_{h,k}$. Moreover, for $k_1, k_2 \in \mathcal{C}_h^T$, $\mathcal{R}_{h,k_1,t} \subseteq \mathcal{R}_{h,k_2,t}$ if $d_{h,k_1} > d_{h,k_2}$. To ensure the spatial shifting of PEV
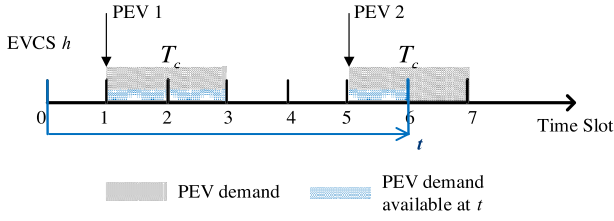
Fig. 2. An illustration for Eq. (8).

requesters under their range anxiety constraint, it holds that $y_{h,k,t} \leq |\mathcal{R}_{h,k,t}|$.

III. PROBLEM FORMULATION

The objective of the PEV power allocation problem is to maximize the overall PEV charging energy for the PEV charging management network over $|\mathcal{T}|$ time slots while weighing the cost of both spatial and temporal PEV demand scheduling. We conduct OPF analysis to prevent overloading caused by a large number of PEV loads plugged into the power distribution system.

To reduce the cost due to spatial demand scheduling, we minimize the difference between the charging power for PEV requesters flowing out from and into EVCS h in the same time slot t due to spatial scheduling. The power difference is denoted by $\Delta_{h,t}$, where

$$\Delta_{h,t} = \left(\sum_{k \in \mathcal{G}} y_{h,k,t} - \sum_{k \in \mathcal{G}} y_{k,h,t} \right) P_c.$$

If $\Delta_{h,t} > 0$, EVCS h serves as a PEV charging source node to transfer PEV power to other EVCSs. If $\Delta_{h,t} < 0$, EVCS h serves as a charging sink node which requires the PEV transferred into it. Note that $\sum_{h \in \mathcal{G}} \sum_{k \in \mathcal{G}} y_{h,k,t} = \sum_{h \in \mathcal{G}} \sum_{k \in \mathcal{G}} y_{k,h,t}$. Therefore, for all EVCSs in the network, a zero-sum constraint should be satisfied, *i.e.*, $\sum_{h \in \mathcal{G}} \Delta_{h,t} = 0$. The constraint ensures that all PEVs are scheduled to be charged by one of EVCSs in the network. No PEV is shifted out of the considered network, and no PEV from outside is shifted into the network.

To analyze the cost of the temporal PEV power shifting, we first formulate the overall PEV charging demand that is available to be allocated at EVCS h in slot t as follows:

$$E_{h,t}(\Delta_h) = \sum_{t'=1}^{t} \min\{t - t' + 1, T_c\} \varpi(|\mathcal{V}_{h,t'}| P_c - \Delta_{h,t'}), \quad (8)$$

where $|\mathcal{V}_{h,t'}| P_c$ represents the maximum charging power for the PEV requester arrived at EVCS h in slot t'. The term Δ_h represents the set $\{\Delta_{h,t}, \forall t\}$. The term $\min\{t - t' + 1, T_c\}$ is the maximum number of time slots in which EVCS may have used to charge a PEV arrived in slot t'. To explain Eq. (8), an example is provided in Fig. 2. Since the charging power is limited by the upper bound P_c, satisfying the charging demand requires at least T_c time slots. The whole demand of PEV 1 is available to be scheduled since the charging process is possible to be finished before slot t by the maximum charging rate. However, for PEV 2, only a part of charging demand can be satisfied by slot t even if the PEV is charged by the

maximum charging rate. It can be seen that $\sum_{t'=1}^{t} \min\{t - t' + 1, T_c\} \varpi(|\mathcal{V}_{h,t'}| P_c - \Delta_{h,t'})$ represents the overall charging demand, which is available to be scheduled, at EVCS h by time slot t. We further formulate the overall PEV charging demand that has to be satisfied at EVCS h in slot t as follows:

$$\bar{E}_{h,t}(\Delta_h) = \begin{cases} \sum_{t'=1}^{t-\bar{T}} T_c \varpi(|\mathcal{V}_{h,t'}| P_c - \Delta_{h,t'}), & \text{if } t > \bar{T} \\ 0, & \text{if } t \leq \bar{T} \end{cases}$$
$$(9)$$

The cost of the temporal PEV power shifting is represented as follows:

$$C_{tem}(\Delta, \mathbf{H}) = \sum_{h \in \mathcal{G}} \sum_{t \in \mathcal{T}} \left[\sum_{t'=1}^{t} H_{h,t'} - E_{h,t}(\Delta_h)/\varpi \right]^2. \quad (10)$$

The cost $C_{tem}(\Delta, \mathbf{H})$ depicts the difference between two energy items, *i.e.*, the overall allocated PEV energy and the overall PEV energy demand at all EVCSs received so far, normalized by the length of a time slot.

Without considering the range anxiety constraint, the power allocation optimization problem can be formulated as follows:

$$\max_{\mathbf{H}, \Delta, \mathbf{V}} \quad \sum_{h \in \mathcal{G}} \sum_{t \in \mathcal{T}} H_{h,t} - \alpha \|\Delta\|_2^2 - \beta C_{tem}(\Delta, \mathbf{H}) \quad (11a)$$

$$\text{s.t.} \sum_{t'=1}^{t} H_{h,t'} \in [\bar{E}_{h,t}(\Delta_h)/\varpi, E_{h,t}(\Delta_h)/\varpi], \quad \forall h, t, \quad (11b)$$

$$\sum_{h \in \mathcal{G}} \Delta_{h,t} = 0, \quad \forall t \quad (11c)$$

$$\text{Tr}(\Psi_{P,h} \mathbf{V}(t)) = P_{h,t} + H_{h,t}, \quad \forall h, t \quad (11d)$$

$$\text{Tr}(\Psi_{Q,h} \mathbf{V}(t)) = Q_{h,t}, \quad \forall h, t \quad (11e)$$

$$\text{Tr}(\mathbf{1}_h (\mathbf{1}_h)^T \mathbf{V}(t)) \in [v_{min}^2, v_{max}^2], \quad \forall h, t \quad (11f)$$

$$P_{0,t}^2 + Q_{0,t}^2 \leq \bar{S}_{0,t}^2 \quad (11g)$$

$$H_{h,t} \in [0, \bar{P}_{h,t} - P_{h,t}], \quad \forall h, t \quad (11h)$$

$$\mathbf{V}(t) \succeq \mathbf{0}, \quad \forall t \quad (11i)$$

$$\text{rank}[\mathbf{V}(t)] = 1. \forall t \quad (11j)$$

The optimization problem (11) presents the overall charging service capacity maximization, which is defined as the overall PEV charging energy offered by EVCSs subtracting the cost of spatial and temporal charging demand scheduling. The non-negative parameter α and β are the factors for the cost of spatial and temporal shifting, respectively. Constraint (11b) shows that the allocated PEV energy at node h cannot be higher than the available PEV power demand arrived in past slots. Consequently, the solution of problem (11) will not allocate the PEV power for the PEV demand that has not arrived yet. Also, the PEVs' charging demand should be satisfied within the expected parking period, *i.e.*, $\bar{T}$. Constraint (11c) suggests that the sum of power flowing among EVCSs should be zero. Power flow constraints in OPF analysis are represented in constraints (11d)-(11j). Main optimization variables include the PEV power allocation result $\mathbf{H}$, the shifting power of

PEV requesters among EVCSs $\boldsymbol{\Delta}$, and the voltage magnitude matrix $\mathbf{V}$.

Problem (11) is a non-convex problem due to constraint (11j). The SDP relaxation technique is applied to drop the rank constraint (11j) such that problem (11) becomes a convex problem and can be solved by a standard interior-point solver [26], [28]. However, the relaxation results in a rank conundrum on the optimality of the results provided by the convexified problem. Several studies investigated the dual gap between the rank-constrained problem and the relaxed problem under the tree network topology [29]–[31]. It is proved that, in a balanced tree power network, as the one considered here, under the assumption that the phase angle differences across a line are controllable and satisfying certain constraints, the global optimality of the rank-constrained problem can be achieved by optimizing the relaxed problem if the power allocation problem is feasible (Theorem 1, [32]).

Remark 1: For the RA scenario, due to the range anxiety limitation, the following upper bound constraint exists for node h receiving the PEV power from all $k \in \mathcal{C}_h^T$:

$$-\sum_{h \in \mathcal{X}_x} \Delta_{h,t} \leq \left(\Big| \bigcup_{\substack{h \in \mathcal{X}_x \\ k \in \mathcal{C}_h^T}} \mathcal{R}_{k,h,t} \Big| - \Big| \bigcup_{h,k \in \mathcal{X}_x} \mathcal{R}_{k,h,t} \Big| \right) P_c, \quad (12)$$

where set $\mathcal{X}_x$ denotes the x-th combination of elements in set $\mathcal{G}$.

The right side of constraint (12) represents the maximum PEV power which can flow into the set of nodes in $\mathcal{X}_x$ under the range anxiety constraint. There are $\sum_{k \in \mathcal{G}} \binom{|\mathcal{G}|}{k}$ number of sets $\mathcal{X}_x$ among $|\mathcal{G}|$ nodes. To simplify the notation, let $T_{x,t}$ represent the negative of the inequality (12)'s left side. Define $\mathbf{T}_t = [T_{1,t}; \ldots; T_{\sum_{k \in \mathcal{G}} \binom{|\mathcal{G}|}{k}, t}]$, and $\boldsymbol{\Delta}_t = [\Delta_{1,t}; \ldots; \Delta_{|\mathcal{G}|,t}]$. The inequality (12) can be reformulated as follows:

$$\mathbf{C}\boldsymbol{\Delta}_t \geq \mathbf{T}_t, \quad (13)$$

where $\mathbf{C}$ is a $\left(\sum_{k \in \mathcal{G}} \binom{|\mathcal{G}|}{k} \times |\mathcal{G}| \right)$ matrix. The element $C_{x,h}$ is one if $h \in \mathcal{X}_x$, otherwise $C_{x,h}$ is zero. From constraint (13), we see the limitation of the PEV maximum traveling range introduces several constraints in the power allocation phase. The power grid needs the knowledge on PEV requesters, such as $\mathbf{T}_t$, to achieve the accurate power allocation results. However, if the number of PEV requesters is high or the distance among EVCSs is short enough, the range anxiety constraint has less influence on the power allocation phase.

Consider the graph $\mathcal{G}_{TN}$. Let $\mathcal{S}$ represent a subset of $\mathcal{G}$, and $\bar{\mathcal{S}} = \mathcal{G} \backslash \mathcal{S}$. Then, we have the following conclusion:

Lemma 1: If the number of PEVs being able to travel from $\mathcal{S}$ to $\bar{\mathcal{S}}$ is $\sum_{h \in \mathcal{S}} |\mathcal{V}_{h,t}|$ for any $\mathcal{S} \neq \mathcal{G}$, the range anxiety constraint (13) can be neglected in the power allocation problem.

Proof: Considering the condition in Lemma 1, if $\bar{\mathcal{S}} = \{k\}$, the maximum number of PEVs can travel to node k is $\sum_{h \in \mathcal{S} \backslash \{k\}} |\mathcal{V}_{h,t}|$. All PEVs from all other nodes can be shifted to node k, such that range anxiety constraints are inactive. Following the above condition, when $\bar{\mathcal{S}}$ has more nodes, the number of PEV requesters which can be shifted into nodes in $\bar{\mathcal{S}}$ is the number of all PEV requesters in its complement set $\mathcal{S}$. Constraint (13) is always satisfied except

the case when $\mathcal{S} = \mathcal{G}$, which is represented by constraint (11c). Under the condition in Lemma 1, no PEV information from the transportation coordinator is required in the power allocation phase. $\square$

IV. DECENTRALIZED OPTIMIZATION IN PEV POWER ALLOCATION

The relaxed power allocation problem (11) is an SDP optimization problem. The classic interior-point method for solving the proposed problem can be time-consuming, especially with a large number of nodes, time slots, and constraints. In addition, in the centralized approach, a central controller should be deployed to gather a vast volume of local parameters for power allocation optimization, such as the information of all PEV requesters for all time slots. Therefore, it is impractical to manage all detailed parameters by a controller when the scale of the power grid is large. Therefore, we introduce a decentralized approach to solve the PEV power allocation problem. PJADMM is a powerful distributed optimization tool, which decomposes the complicated centralized problem into multiple subproblems, and those subproblems can be determined with local solvers in parallel. Compared with conventional ADMM, PJADMM combines the proximal term $\frac{\tau}{2}||x_i - x_i^t||^2$ in the primal problem to guarantee strict convexity with multiple constraints, and results could converge under much milder conditions [33].

Problem (11) is fully separable except constraints related to $\mathbf{V}(t)$ and $\Delta_{h,t}$. To split those constraints, we define several new local and global variables. Local variables are solved by nodes, and global variables are shared among nodes. For constraint (11i), we introduce two variables, *i.e.* $\hat{\mathbf{V}}_h(t)$ and $\mathbf{W}_h(t)$. The variable $\hat{\mathbf{V}}_h(t)$ is the global variable containing the voltage magnitude information on node h and its adjacent nodes in the grid topology, which is the sub-matrix of $\mathbf{V}(t)$ for node h. For example, for node 2 in Fig. 1(c), the variable $\hat{\mathbf{V}}_2(t)$ is:

$$\hat{\mathbf{V}}_2(t) = \begin{bmatrix} v_{1,t}v_{1,t}^* & v_{1,t}v_{2,t}^* & v_{1,t}v_{5,t}^* & v_{1,t}v_{7,t}^* \\ v_{2,t}v_{1,t}^* & v_{2,t}v_{2,t}^* & v_{2,t}v_{5,t}^* & v_{2,t}v_{7,t}^* \\ v_{5,t}v_{1,t}^* & v_{5,t}v_{2,t}^* & v_{5,t}v_{5,t}^* & v_{5,t}v_{7,t}^* \\ v_{7,t}v_{1,t}^* & v_{7,t}v_{2,t}^* & v_{7,t}v_{5,t}^* & v_{7,t}v_{7,t}^* \end{bmatrix}$$

The variable $\mathbf{W}_h(t)$ is the corresponding voltage magnitude matrix solved by node h locally. Moreover, denote the mean of local variables $\{\Delta_{h,t}, \forall h\}$ as $\bar{\Delta}_t$, *i.e.*, $\bar{\Delta}_t = (1/|\mathcal{G}|) \sum_{h \in \mathcal{G}} \Delta_{h,t}$. The corresponding constraint (11c) can be transformed to compute local $\Delta_{h,t}$ so that the average, $\bar{\Delta}_t$, is zero. For the *RA* scenario, we consider a constraint set $\mathcal{C}_R$, where $\mathcal{C}_R = \{\boldsymbol{\Delta}_t \in \mathbb{R}^{|\mathcal{G}|} | \mathbf{C}\boldsymbol{\Delta}_t \geq \mathbf{T}_t\}$. After introducing above variables, the optimization problem (11) is rewritten as follows:

$$\max_{\mathbf{H}, \boldsymbol{\Delta}, \mathbf{W}} \sum_{h \in \mathcal{G}} \sum_{t \in \mathcal{T}} H_{h,t} - \alpha\|\boldsymbol{\Delta}\|_2^2 - \beta C_{tem}(\boldsymbol{\Delta}, \mathbf{H}) \quad (14a)$$

$$\text{s.t. } \bar{\Delta}_t = 0, \forall t \quad (14b)$$

$$\text{Tr}\left(\boldsymbol{\Psi}_{P,h} \mathbf{W}_h(t)\right) = P_{h,t} + H_{h,t}, \quad \forall h, \ t \quad (14c)$$

$$\text{Tr}\left(\boldsymbol{\Psi}_{Q,h} \mathbf{W}_h(t)\right) = Q_{h,t}, \quad \forall h, \ t \quad (14d)$$

$$\text{Tr}\left(\mathbf{1}_h(\mathbf{1}_h)^T \mathbf{W}_h(t)\right) \in [v_{min}^2, v_{max}^2], \quad \forall h, \ t \quad (14e)$$

$$\mathbf{W}_h(t) \succeq \mathbf{0}, \quad \forall h, \ t \tag{14f}$$

$$Re\{\mathbf{W}_h(t)\} = Re\{\hat{\mathbf{V}}_h(t)\}, \forall h, t \tag{14g}$$

$$Im\{\mathbf{W}_h(t)\} = Im\{\hat{\mathbf{V}}_h(t)\}, \quad \forall h, \ t \tag{14h}$$

$$(11b), (11g), (11h),$$

$$(14b), \text{ for the } RA \text{ scenario.}$$

The partial quadratically-augmented Lagrangian of problem (14) is shown in Eq. (15):

$$\Gamma(\mathbf{H}, \mathbf{\Delta}, \mathbf{W}, \boldsymbol{z}, \boldsymbol{u})$$
$$= -\sum_{h \in \mathcal{G}} \sum_{t \in \mathcal{T}} H_{h,t} + \alpha \|\mathbf{\Delta}\|_2^2 + \beta C_{tem}(\mathbf{\Delta}, \mathbf{H})$$

$$+ \sum_{h \in \mathcal{G}} \sum_{t \in \mathcal{T}} \Big\{ u_{1,h,t} [\sum_{t'=1}^{t} H_{h,t'} - E_{h,t}(\mathbf{\Delta}_h)/\varpi - z_{1,h,t}]$$

$$+ \frac{\rho_1}{2} [\sum_{t'=1}^{t} H_{h,t'} - E_{h,t}(\mathbf{\Delta}_h)/\varpi - z_{1,h,t}]^2 \Big\}$$

$$+ \sum_{h \in \mathcal{G}} \sum_{t \in \mathcal{T}} \Big\{ u_{2,h,t} [\sum_{t'=1}^{t} H_{h,t'} - \bar{E}_{h,t}(\mathbf{\Delta}_h)/\varpi - z_{2,h,t}]$$

$$+ \frac{\rho_2}{2} [\sum_{t'=1}^{t} H_{h,t'} - \bar{E}_{h,t}(\mathbf{\Delta}_h)/\varpi - z_{2,h,t}]^2 \Big\}$$

$$+ \sum_{h \in \mathcal{G}} \sum_{t \in \mathcal{T}} \Big\{ u_{3,h,t}(H_{h,t} - z_{3,h,t}) + \frac{\rho_3}{2}(H_{h,t} - z_{3,h,t}$$

$$+ u_{3,h,t})^2 \Big\} + \sum_{t \in \mathcal{T}} \Big\{ u_{4,t}\bar{\Delta}_t + \frac{\rho_4}{2}(\bar{\Delta}_t)^2 \Big\}$$

$$+ \sum_{h \in \mathcal{G}} \sum_{t \in \mathcal{T}} \Big\{ u_{5,h,t}[\mathrm{Tr}\,(\mathbf{\Psi}_{P,h}\mathbf{W}_h(t)) - P_{h,t} - H_{h,t}]$$

$$+ \frac{\rho_5}{2}[\mathrm{Tr}\,(\mathbf{\Psi}_{P,h}\mathbf{W}_h(t)) - P_{h,t} - H_{h,t}]^2 \Big\}$$

$$+ \sum_{h \in \mathcal{G}} \sum_{t \in \mathcal{T}} \mathrm{Tr}\,\big[\mathbf{u}_{6,h,t}^T(Re\{\mathbf{W}_h(t)\} - Re\{\hat{\mathbf{V}}_h(t)\})\big]$$

$$+ \frac{\rho_6}{2} \sum_{h \in \mathcal{G}} \sum_{t \in \mathcal{T}} \|Re\{\mathbf{W}_h(t)\} - Re\{\hat{\mathbf{V}}_h(t)\}\|_F^2$$

$$+ \sum_{h \in \mathcal{G}} \sum_{t \in \mathcal{T}} \mathrm{Tr}\,\big[\mathbf{u}_{7,h,t}^T(Im\{\mathbf{W}_h(t)\} - Im\{\hat{\mathbf{V}}_h(t)\})\big]$$

$$+ \frac{\rho_7}{2} \sum_{h \in \mathcal{G}} \sum_{t \in \mathcal{T}} \|Im\{\mathbf{W}_h(t)\} - Im\{\hat{\mathbf{V}}_h(t)\}\|_F^2$$

$$+ \sum_{t \in \mathcal{T}} \rho_R \Big\{ \mathbf{u}_{8,t}^T(\mathbf{C}\mathbf{\Delta}_t - \mathbf{z}_{8,t}) + \frac{\rho_8}{2} \|\mathbf{C}\mathbf{\Delta}_t - \mathbf{z}_{8,t}\|_2^2 \Big\}. \tag{15}$$

The variables $\{(\mathbf{u}_1, \mathbf{u}_2), \mathbf{u}_3, \mathbf{u}_4, \mathbf{u}_5, \mathbf{u}_6, \mathbf{u}_7, \mathbf{u}_8\}$ are the penalty term transformed by dual variables associated with constraints (11b), (11h), (14b), (14c), (14g), (14h), and (13), respectively. The auxiliary variables $\{(\mathbf{z}_1, \mathbf{z}_2), \mathbf{z}_3, \mathbf{z}_8\}$ illustrate inequality constraints in (11b), (11h), and (13), respectively. Parameters $\{\rho_1, \ldots, \rho_8\}$ are positive constants. The indicator ρ_R is one for the *RA* scenario, and ρ_R is zero for the *free traveling* scenario, in which range anxiety is not considered.

In order to reduce the computation scale of the SDP problem, we decompose problem (14) into multiple subproblems by PJADMM and determine each variable by an individual subproblem at the node level in an iterative manner.

The subproblem for solving PEV charging power allocation, *i.e.*, $H_{h,t}$, is organized in the following problem:

$$\min_{\{H_{h,t}, \forall t\}} \sum_{t \in \mathcal{T}} \Big\{ -H_{h,t} + \beta \Big[\sum_{t'=1}^{t} H_{h,t'} - E_{h,t}(\mathbf{\Delta}_h^{(s-1)})/\varpi \Big]^2$$

$$+ (u_{1,h,t}^{(s-1)} + u_{2,h,t}^{(s-1)})(\sum_{t'=1}^{t} H_{h,t'}) + \frac{\rho_1}{2} [\sum_{t'=1}^{t} H_{h,t'}$$

$$- E_{h,t}(\mathbf{\Delta}_h^{(s-1)})/\varpi - z_{1,h,t}^{(s-1)}]^2 + \frac{\rho_2}{2} [\sum_{t'=1}^{t} H_{h,t'}$$

$$- \bar{E}_{h,t}(\mathbf{\Delta}_h^{(s-1)})/\varpi - z_{2,h,t}^{(s-1)}]^2 + u_{3,h,t}^{(s-1)} H_{h,t}$$

$$+ \frac{\rho_3}{2}(H_{h,t} - z_{3,h,t}^{(s-1)} + u_{3,h,t}^{(s-1)})^2 - u_{5,h,t}^{(s-1)} H_{h,t}$$

$$+ \frac{\rho_5}{2}[\mathrm{Tr}\,(\mathbf{\Psi}_{P,h}\mathbf{W}_h^{(s-1)}(t)) - P_{h,t} - H_{h,t}]^2$$

$$+ \frac{\tau}{2}(H_{h,t} - H_{h,t}^{(s-1)})^2 \Big\}, \tag{16}$$

where $x^{(s-1)}$ is the result of the variable x obtained by iteration $s-1$, and the constant terms are omitted. The subproblem for calculating the power difference, *i.e.*, $\Delta_{h,t}$, is organized in the following problem:

$$\min_{\{\Delta_{h,t}, \forall t\}} \sum_{t \in \mathcal{T}} \Big\{ \alpha \Delta_{h,t}^2 + \beta \Big[\sum_{t'=1}^{t} H_{h,t'}^{(s-1)} - E_{h,t}(\mathbf{\Delta}_h)/\varpi \Big]^2$$

$$- u_{1,h,t}^{(s-1)}[E_{h,t}(\mathbf{\Delta}_h)/\varpi] + \frac{\rho_1}{2} [\sum_{t'=1}^{t} H_{h,t'}^{(s-1)}$$

$$- E_{h,t}(\mathbf{\Delta}_h)/\varpi - z_{1,h,t}^{(s-1)}]^2 - u_{2,h,t}^{(s-1)}[\bar{E}_{h,t}(\mathbf{\Delta}_h)/\varpi]$$

$$+ \frac{\rho_2}{2} [\sum_{t'=1}^{t} H_{h,t'}^{(s-1)} - \bar{E}_{h,t}(\mathbf{\Delta}_h)/\varpi - z_{2,h,t}^{(s-1)}]^2$$

$$+ u_{4,t}^{(s-1)}\Delta_{h,t} + \frac{\rho_4}{2}(\Delta_{h,t} - \Delta_{h,t}^{(s-1)} + \bar{\Delta}_t^{(s-1)})^2$$

$$+ \rho_R \Big\{ (\mathbf{u}_{8,t}^{(s-1)})^T[\mathbf{C}(:,h)\Delta_{h,t}/|\mathcal{G}|] + \frac{\rho_8}{2} \|\mathbf{C}\mathbf{\Delta}_t^{(s-1)}$$

$$/|\mathcal{G}| + \mathbf{C}(:,h)(\Delta_{h,t} - \Delta_{h,t}^{(s-1)}) - \mathbf{z}_{8,t}^{(s-1)}/|\mathcal{G}|\|_2^2 \Big\}$$

$$+ \frac{\tau}{2}(\Delta_{h,t} - \Delta_{h,t}^{(s-1)})^2 \Big\}. \tag{17}$$

The subproblem for determining the voltage magnitude matrix, *i.e.*, $\mathbf{W}_h(t)$, is organized in the following problem:

$$\min_{\substack{\{\mathbf{W}_h(t) \succeq \mathbf{0} \\ , \forall t\}}} \sum_{t \in \mathcal{T}} \Big\{ u_{5,h,t}^{(s-1)}(\mathrm{Tr}\,(\mathbf{\Psi}_{P,h}\mathbf{W}_h(t)))$$

$$+ \frac{\rho_5}{2}[\mathrm{Tr}\,(\mathbf{\Psi}_{P,h}\mathbf{W}_h(t)) - P_{h,t} - H_{h,t}^{(s-1)}]^2$$

$$+ \mathrm{Tr}\,\big\{ (u_{6,h,t}^{(s-1)})^T(Re\{\mathbf{W}_h(t)\} - Re\{\hat{\mathbf{V}}_h(t)^{(s-1)}\}) \big\}$$

$$+ \frac{\rho_6}{2} \|Re\{\mathbf{W}_h(t)\} - Re\{\hat{\mathbf{V}}_h(t)^{(s-1)}\}\|_F^2$$

$$+ \mathrm{Tr}\,\big\{ (u_{7,h,t}^{(s-1)})^T(Im\{\mathbf{W}_h(t)\} - Im\{\hat{\mathbf{V}}_h(t)^{(s-1)}\}) \big\}$$

$$+ \frac{\rho_7}{2} \|Im\{\mathbf{W}_h(t)\} - Im\{\hat{\mathbf{V}}_h(t)^{(s-1)}\}\|_F^2$$

$$+ \frac{\tau_v}{2} \|\mathbf{W}_h(t) - \mathbf{W}_h(t)^{(s-1)}\|_F^2 \Big\}$$

$$\text{s.t. } (11g), (14d), (14e). \tag{18}$$

The decomposition process is provided in Appendix. For each subproblem, we add the proximal term to ensure the convergence for the multi-constraint problem [33], where τ and τ_v are positive parameters. The full PJADMM algorithm is illustrated in Algorithm 1. The corresponding dual and auxiliary variables updates for solving the subproblems are also presented in Algorithm 1.

Lemma 2: If the initial value of dual variables $\boldsymbol{u}_4^0$ and $\boldsymbol{u}_8^0$ are unified among all nodes, the two dual variables are not required to be shared among nodes in the PJADMM algorithm though they contain the information of all nodes in the considered network.

Proof: When computing $\boldsymbol{u}_4^{(s-1)}$, the following information are required: $\{\bar{\Delta}_t^{(s-1)}, \forall t\}$ and $\boldsymbol{u}_4^{(s-2)}$. Since $\Delta_{h,t}$ is updated and broadcasted at the beginning of each iteration, $\boldsymbol{u}_4$ can be updated at each node individually by the historical value of $\boldsymbol{u}_4$. Likewise, $\boldsymbol{u}_8$ can be updated individually in a similar way. □

In our power allocation algorithm, the optimum result can be achieved in a distributed manner by sharing only two variables: $\Delta_{h,t}$ among all nodes and $\mathbf{W}_h(t)$ among adjacent nodes in the grid topology. In Algorithm 1, firstly, two global variables, $\Delta_{h,t}$ and $\hat{\mathbf{V}}_h(t)$, are calculated by the two variables, $\Delta_{h,t}$ and $\mathbf{W}_h(t)$, shared among nodes in Step (1). Step (1b) computes the global matrix for node h, $\hat{\mathbf{V}}_h(t)$. Each element in the global matrix $\hat{\mathbf{V}}_h(t)$ is the average of elements with the same voltage information in local variables $\mathbf{W}_k(t)$. Set O_{i^*,j^*} is a subset containing node h and the adjacent nodes of node h. Node k is in set O_{i^*,j^*} only if its local matrix, $\mathbf{W}_k(t)$, has the element (i', j') representing the same voltage information with the element (i^*, j^*) in local matrix $\mathbf{W}_h(t)$ corresponding to global matrix $\mathbf{V}(t)$. Steps (2)-(4) solve subproblems in parallel. Local variables and dual variables are computed by individual nodes iteratively until the stop criterion is satisfied.

In the proposed algorithm, local parameters and variables, such as active power demand $P_{h,t}$ and the PEV power allocation result $H_{h,t}$, are not required to be passed among distribution nodes. Furthermore, the SDP optimization suffers from high time complexity. In the current SDP solvers, interior-point methods have been adopted. The time complexity of solving SDP problem (14) in the centralized manner is estimated as $O(T|\mathcal{G}|^{4.5})$ or worse [34]. In the decentralized approach, problem (14) is converted into several linear optimization problems, *i.e.*, problem (16) and problem (17), and one SDP problem with fewer variables and constraints, *i.e.*, problem (18). The subproblems are solved by each charging station distributively. The time complexity in solving the decomposed SDP problem can be estimated as $O(T|\mathcal{C}_h^G|^{4.5})$ for a charging station, and each charging station solves the subproblem in parallel. The computation scale in problem solving is reduced significantly, especially when the number of nodes in the network is large.

V. PARAMETER ESTIMATION FOR PEV REQUESTERS

In our algorithm, all PEV charging information for the optimization period $\mathcal{T}$ is considered to be available. However, due to limited communication distance of V2I communications and charging demand uncertainty, it can be difficult for EVCSs to obtain the exact charging information of PEV requesters

---

Algorithm 1 Proximal Jacobian ADMM Algorithm for Power Allocation

1: Iteration $s = 1$. Initialize variables $(\mathbf{H}, \boldsymbol{\Delta}, \mathbf{W}, \boldsymbol{z}, \boldsymbol{u})^0 = (\boldsymbol{0}, \boldsymbol{0}, \boldsymbol{0}, \boldsymbol{0}, \boldsymbol{0})$, and $\Gamma(\mathbf{H}, \boldsymbol{\Delta}, \mathbf{W}, \boldsymbol{z}, \boldsymbol{u})^0 = 0$.

2: **for** Each bus $h = 1 : N$ **do**
   (1) Update Global Variables
   (1a) Update $\bar{\Delta}_t^{(s-1)} = \frac{1}{|\mathcal{G}|} \sum_{h \in \mathcal{G}} \Delta_{h,t}^{(s-1)}, \forall t$.
   (1b) $\hat{\mathbf{V}}_h(t)_{[i^*,j^*]}^{(s-1)} = \frac{1}{|O_{i^*,j^*}|} \sum_{k \in O_{i^*,j^*}} \mathbf{W}_k(t)_{[i^*,j^*]}^{(s-1)}$, $O_{i^*,j^*} \subseteq \mathcal{C}_h^G \cup h, \forall t$

   (2) Update Auxiliary Variables for the Past Iteration
   (2a) $z_{1,h,t}^{(s-1)} = \Pi_{\mathbf{R}^-}\{\sum_{t'=1}^t H_{h,t'}^{(s-1)} - E_{h,t}(\boldsymbol{\Delta}_h^{(s-1)})/\varpi + u_{1,h,t}^{(s-1)}/\rho_1\}, \forall t$
   (2b) $z_{2,h,t}^{(s-1)} = \Pi_{\mathbf{R}^+}\{\sum_{t'=1}^t H_{h,t'}^{(s-1)} - \bar{E}_{h,t}(\boldsymbol{\Delta}_h^{(s-1)})/\varpi + u_{2,h,t}^{(s-2)}/\rho_2\}, \forall t$
   (2c) $z_{3,h,t}^{(s-1)} = \Pi_{\mathbf{C}_1}\{H_{h,t}^{(s-1)} + u_{3,h,t}^{(s-2)}/\rho_3\}$, where $\mathbf{C}_1 = [0, \bar{P}_{h,t} - P_{h,t}], \forall t$
   (2d) $\mathbf{z}_{8,t}^{(s-1)} = \Pi_{\mathbf{C}_2}\{\mathbf{C}\boldsymbol{\Delta}_t^{(s-1)} + \mathbf{u}_{8,t}^{(s-2)}/\rho_8\}$, where $\mathbf{C}_2 = [\mathbf{T}_t, \boldsymbol{0}], \forall t$

   (3) Update Dual Variables for the Past Iteration
   (3a) $u_{1,h,t}^{(s-1)} = \rho_1(\sum_{t'=1}^t H_{h,t'}^{(s-1)} - E_{h,t}(\boldsymbol{\Delta}_h^{(s-1)}))/\varpi - z_{1,h,t}^{(s-1)} + u_{1,h,t}^{(s-2)}, \forall t$
   (3b) $u_{2,h,t}^{(s-1)} = \rho_2(\sum_{t'=1}^t H_{h,t'}^{(s-1)} - \bar{E}_{h,t}(\boldsymbol{\Delta}_h^{(s-1)}))/\varpi - z_{2,h,t}^{(s-1)} + u_{2,h,t}^{(s-2)}, \forall t$
   (3c) $u_{3,h,t}^{(s-1)} = \rho_3(H_{h,t}^{(s-1)} - z_{3,h,t}^{(s-1)}) + u_{3,h,t}^{(s-2)}, \forall t$
   (3d) $u_{4,t}^{(s-1)} = \rho_4\bar{\Delta}_t^{(s-1)} + u_{4,t}^{(s-2)}, \forall t$
   (3e) $u_{5,h,t}^{(s-1)} = \rho_5[\text{Tr}(\boldsymbol{\Psi}_{P,h}\mathbf{W}_h(t)^{(s-1)}) - P_{h,t} - H_{h,t}^{(s-1)}] + u_{5,h,t}^{(s-2)}, \forall t$
   (3f) $u_{6,h,t}^{(s-1)} = \rho_6(Re\{\mathbf{W}_h(t)^{(s-1)}\} - Re\{\hat{\mathbf{V}}_h(t)^{(s-1)}\}) + u_{6,h,t}^{(s-2)}, \forall t$
   (3g) $u_{7,h,t}^{(s-1)} = \rho_7(Im\{\mathbf{W}_h(t)^{(s-1)}\} - Im\{\hat{\mathbf{V}}_h(t)^{(s-1)}\}) + u_{7,h,t}^{(s-2)}, \forall t$
   (3h) $\mathbf{u}_{8,t}^{(s-1)} = \rho_8(\mathbf{C}\boldsymbol{\Delta}_t^{(s-1)} - \mathbf{z}_{8,t}^{(s-1)}) + \mathbf{u}_{8,t}^{(s-2)}$, if $\rho_R = 1$.
   (4) Update primal variables by solving (16)-(18)

3: **end for**
4: Nodes exchange variables $\Delta_{h,t}^{(s)}$ and $W_h(t)^{(s)}$.
5: Find Γ^s by Eq. (15), and update $s = s + 1$.
6: Repeat 2-5 until either $|\Gamma^{(s)} - \Gamma^{(s-1)}|^2 \leq \xi$, or s reaches the maximum iteration value.

---

arriving in the future. Therefore, we discuss parameter estimation for PEV requesters in this section.

There are two main parameters related to PEVs that EVCSs need to obtain in the optimization process: $\mathcal{V}_{h,t}$ and $\mathcal{R}_{h,t}$. The size of set $\mathcal{V}_{h,t}$, *i.e.*, the number of PEV requesters local to h arriving in slot t, can be modelled by a Poisson distribution [12], [21], [35], [36]. However, the distribution to illustrate the range anxiety of the PEV requesters, represented by $\mathcal{R}_{h,k,t}$, has not been well investigated. Depends on the EVCS location, the types of PEVs being served at the EVCS may vary. For example, EVCSs located in rural areas are more likely to serve PEVs with high battery capacities, such as electric trucks. Such PEVs have a higher chance to

possess enough remaining energy to travel to another EVCS. In contrast, EVCSs located at an urban area may more likely to serve PEVs with low battery capacities, such as private PEVs for commuting, which has lower flexibility for spatial coordination. Therefore, to estimate the spatial coordinating ability for PEV requesters, we adopt a non-parametric density estimation method, *i.e.*, Gaussian kernel density estimation, to determine the distribution of PEV requesters' maximum traveling distance for spatial shifting among EVCSs. The historical PEV charging profile, including the maximum traveling distance D_e and the arrival time, is collected by individual EVCS. By excavating the relation between the arrival time and the maximum traveling distance D_e in various EVCSs, we could find the probability that the PEV requester arriving in a particular time slot at an EVCS can be shifted to another specific EVCS. Then, the size of set $\mathcal{R}_{h,k,t}$ can be obtained by the estimated probability.

Denote the average PEV arrival rate at EVCS h in time slot t as $\lambda_{h,t}$. Consider that the distribution of the number of PEV entering an EVCS is independent on the charging properties of PEVs. Before estimating the distribution of the maximum traveling distances of PEV requesters, the EVCS needs to gather enough samples on the charging profile of the PEVs requesters request to the EVCS in the past. The historical charging profile of those PEVs e' is denoted by $s_{e'} = [s_{e'}^t, s_{e'}^l]$, where $s_{e'}^t$ represents the arriving time instant of PEV e', and $s_{e'}^l$ represents the maximum travelling distance of PEV e'. The set of PEV requesters arrived in the past is denoted by $\mathcal{I}$ and is collected to estimate the distribution of the maximum traveling distance for the PEV arrived in a particular time instant, where the probability density function for the PEV arriving in time instant $\dot{t}$ with the maximum traveling distance of l is denoted as $f(\dot{t}, l)$.

In order to compute $f(\dot{t}, l)$, we consider the uniform kernel case at first. Consider a small region R which is a rectangle area with side length of σ_t and σ_l. Then, the number of samples falling within the region is counted by following function:

$$C(s_{e'}^t, s_{e'}^l; R) = \begin{cases} 1, & \text{if } \max\left\{ \dfrac{||s_{e'}^t - \dot{t}||}{\sigma_t}, \dfrac{||s_{e'}^l - l||}{\sigma_l} \right\} \leq \dfrac{1}{2} \\ 0, & \text{otherwise,} \end{cases}$$

$$(19)$$

where $(\dot{t}, l)$ is the central point of area R. Thus, for a large N, the general expression for non-parametric density estimation for the uniform kernel is [37]

$$\hat{f}(\dot{t}, l) = \frac{1}{|\mathcal{I}|\sigma_t \sigma_l} \sum_{e' \in \mathcal{I}} C(s_{e'}^t, s_{e'}^l; R). \tag{20}$$

The term $\hat{f}(\dot{t}, l)$ is the estimated distribution, which represents the likeliness of a sample falling into the rectangle window. Moreover, to smooth the shape of the kernel and develop a continuous probability distribution function, we further improve the uniform kernel into a smooth Gaussian kernel. The estimated distribution $\hat{f}(\dot{t}, l)$ can be formulated as follows:

$$\hat{f}(\dot{t}, l) = \frac{1}{|\mathcal{I}|\sqrt{\sigma_t \sigma_l}} \sum_{e' \in \mathcal{I}} \frac{1}{2\pi} e^{-\left[\frac{(s_{e'}^t - \dot{t})^2}{2\sigma_t} + \frac{(s_{e'}^l - l)^2}{2\sigma_l} \right]}. \tag{21}$$

In (21), σ_t and σ_l represent the bandwidth of the Gaussian kernel rather than the side length of the uniform kernel. To improve the estimation quality, the proper bandwidth is required to be selected to minimize the error between the estimated density and the true density. The bandwidth selection is critical since it determines the shape of the corresponding estimator. A sharp estimator with low bandwidth would result in high variance on density estimation. On the other hand, an overly smooth estimator with high bandwidth would reduce the accuracy of estimation. In this work, we adopt the maximum likelihood cross-validation method [37] to determine the bandwidth σ_t and σ_l as follows:

$$[\sigma_t, \sigma_l] = \arg\max \left\{ \frac{1}{|\mathcal{I}|} \sum_{e' \in \mathcal{I}} \log \hat{f}_{-e'}(s_{e'}^t, s_{e'}^l) \right\}, \tag{22}$$

where $\hat{f}_{-e'}(\dot{t}, l)$ is the estimated distribution without considering user e. Let the term $p_{h,k,t}$ denote the probability of the case in which the PEV requester arriving at station h in time slot t can be shifted to station k. By the above probability density function of the PEV requesters' maximum traveling distance, we can have

$$p_{h,k,t} = \int_{\dot{t}=t\varpi}^{(t+1)\varpi} \int_{l=d_{h,k}}^{\infty} \hat{f}(\dot{t}, l) \, dt \, dl. \tag{23}$$

Then the average number of PEV requesters, which is local to h and can be shifted to k in slot t, can be formulated as follows:

$$\gamma_{h,k,t} = p_{h,k,t}\lambda_{h,t}. \tag{24}$$

During the optimization process, the size of sets $\mathcal{V}_{h,t}$ and $\mathcal{R}_{h,k,t}$ can be estimated by $\lambda_{h,t}$ and $\gamma_{h,k,t}$, respectively.

VI. SIMULATION RESULTS

A. Parameter Settings

A five-node network and a ten-node network are shown in Fig. 3(a) and 3(b), respectively. When implemented in a grid with a tree topology, the proposed approach can guarantee the global optimality [29]–[31]. The solid line in the figures represents the power connection. For the five-node network, the dashed line represents the bi-directed transportation connection. For the ten-node network, the bi-directed transportation connection is shown as Fig. 3(c), which is a real transportation network topology in Waterloo, ON, Canada. The parameter settings are given in Table II. We consider three cases in the simulation: *free traveling*, *RA*, and greedy case. For the first two cases, PEV charging energy is allocated by the proposed strategy. For the greedy case, the maximum PEV charging energy is allocated according to the upper bound $\bar{P}_{h,t}$ without any spatial shifting scheduling.

We implement the PEV charging power allocation approach in the five-node scenario to evaluate the charging capacity improvement. In the transportation layer, suppose node 1 to 3 have 10 PEV requesters for a time slot at each node, and we vary the number of PEV requesters at node 4 from 5 to 50 to test the charging service capacity in the power distribution system. Parameters α and β are 0.1 and 0, respectively.

TABLE II

SIMULATION PARAMETERS

Parameter	Value	Five-node Network		Ten-node Network	
		Parameter	Value	Parameter	Value
θ_{max}	5 kM	v_{min}	0.974 p.u.	v_{min}	0.92 p.u.
S_{base}	1 MVA	$P_{h,t}$	0.5 p.u.	T	48
$|v_{0,t}|, \forall t$	4.16 kV	$Q_{h,t}$	0.25 p.u.	Line Impedance [26]	$\bar{z}_{0,1} = 0.0693+0.2036i; \bar{z}_{1,2} = 0.0312 + 0.1003i;$
P_c	0.045 p.u.	T	2		$\bar{z}_{3,4} = 0.0316 + 0.0847i; \bar{z}_{1,3} = 0.0312 +0.1003i;$ $\bar{z}_{2,5} = 0.0675 + 0.2096i; \bar{z}_{5,6} = 0.0307 + 0.0770i;$
T_c	1	$\bar{z}_{h,k}, \forall h, k \in \mathcal{C}_h^G$	0.05+0.05i p.u.		$\bar{z}_{2,7} = 0.0316 +0.0847i; \bar{z}_{7,8} = 0.0307 + 0.0770i;$ $\bar{z}_{8,9} = 0.0683 + 0.2070i$

TABLE III

TIME-VARIANT TRAFFIC INPUT RATE FOR TYPE 1 TO TYPE 3 TRAFFIC (UNIT: VEH/HOUR)

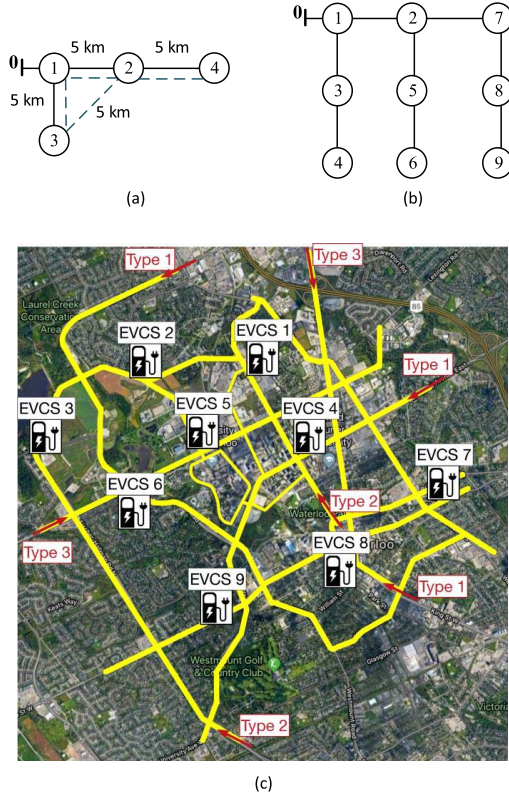| Time	Vehicle Composition (Truck/Bus/LD/SD)	8:00	10:00	12:00	14:00	16:00	18:00	20:00	22:00	0:00	2:00	4:00	6:00
Type 1	0%/10%/45%/45%	789	728	573	385	224	122	88	122	224	385	573	728
Type 2	0%/10%/45%/45%	223	385	573	728	789	728	573	385	224	118	86	121
Type 3	40%/40%/10%/0%	138	77	55	77	141	242	361	458	469	458	360	241

Fig. 3. (a) The five-node network topology. (b) The ten-node network topology. (c) A snap shot of the simulation region with signing the simulated roads in yellow.

For the *free-traveling* case, the PEV can be shifted to any node without considering the range anxiety. For the *RA* case, since the distances between non-adjacent EVCSs are over the threshold θ_{max}, we consider that all PEVs can only travel to adjacent EVCSs of their local EVCS.

In the ten-node network scenario, line impedances have the same setting in [26]. We consider power allocation for a whole day starting at 8:00. The number of the time slots T is 48,

i.e., $\varpi = 30$ min. The power profile excluding PEV loads in a day is adopted from [38], where nodes are classified into residential nodes (nodes 4, 6-9), retail nodes (nodes 3, 5), and industrial nodes (nodes 1, 2). We consider two base load patterns. In *pattern A*, there are 250 residential/retail/industrial units in the corresponding nodes. In *pattern B*, there are 300 residential, 120 retail, and 50 industrial units in the corresponding nodes. To estimate the PEV information, we simulate the PEV traffic with VISSIM in an 8km×10km region. The vehicle input points and EVCS locations are indicated in Fig. 3(c). Each node is connecting a corresponding numbered EVCS. The distance among nine EVCSs is measured from the real simulation region from Google map. We consider that four kinds of vehicles: bus, truck, private vehicle for long distance commuting (LD), and private vehicle for short distance commuting (SD), compose three types of input traffic as given in Table III. The time-variant traffic input rate of the three traffic types for a day is also given in Table III. Among all vehicles, the PEV penetration rate is in 5%. The battery capacity, *i.e.*, B_e, for the corresponding four kinds of PEVs are [200, 120, 110, 80] kWh, and the traveling energy consumption rate, *i.e.*, p_e^{con}, are [0.2, 0.2, 0.16, 0.16] KWh/km. The cost rate parameter η is 50. The PEV state of charge follows a distribution made by an exponential distribution with mean $1/\mu = 40\%$ under the condition that $20\% \leq \text{SoC}_e \leq 100\%$. Consider 50% of PEVs enter the EVCS when the vehicles are passing by. Since the range anxiety of PEV is considered in this part, only *RA* and greedy case are investigated.

B. Power Allocation for the Four-Node Network

The minimum voltage magnitude with the various number of PEV requesters at node 4 is shown in Fig. 4(a). The voltage drop requirement in our approach is not violating the requirement with the increasing PEV charging requests, while the greedy case cannot maintain the voltage drop constraint when the number of PEV requesters is higher than 10 at node 4.
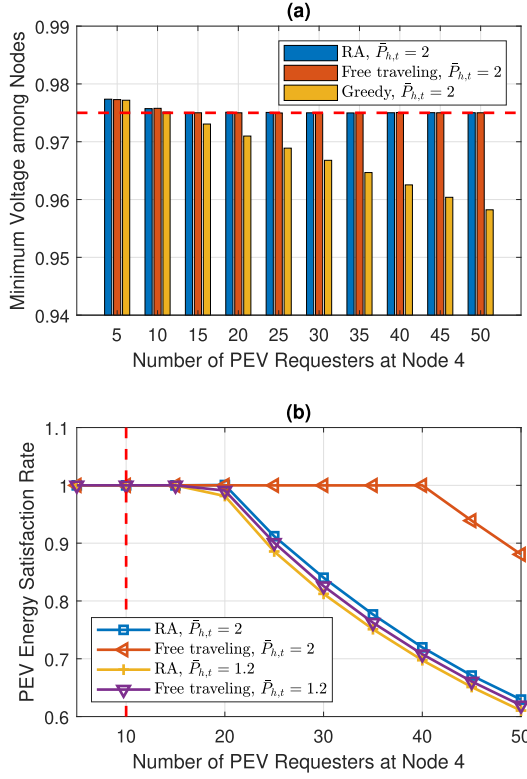
Fig. 5. The convergence performance in terms of the stop criterion for the *RA* case.

Fig. 4. (a) The minimum voltage magnitude with the various number of PEV requesters at node 4. (b) Overall PEV demand satisfaction percentage.

Fig. 6. (a) Historical PEV profile at EVCS 1. (b) The estimated distribution of PEV requesters' maximum traveling range at EVCS 1. (c) Historical PEV profile at EVCS 5. (d) The estimated distribution of PEV requesters' maximum traveling range at EVCS 5.

Correspondingly, to measure the portion of the allocated PEV demand, we define a satisfaction rate (SR) in slot t as follows:

$$\text{SR}_t = \frac{\sum_{h \in \mathcal{G}} \sum_{t'=1}^{t} H_{h,t'}}{\sum_{h \in \mathcal{G}} \sum_{t'=1}^{t} \min\{t - t' + 1, T_c\} |\mathcal{V}_{h,t'}| P_c}, \quad (25)$$

which represents the ratio between the allocated PEV power and PEV power demand in the past slots for whole network. When the satisfaction percentage in slot t is equal to one, all PEV charging demand arrived by slot t has been satisfied. The results of PEV demand satisfaction percentage are shown in Fig. 4(b), in which the constraint $\bar{P}_{h,t}$ is also considered. Complying power distribution system constraints, our approach can allocate more charging demand and thereby improve service capacity significantly compared with the greedy case in which the maximum number of PEV requesters allowed at node 4 is 10 as mentioned above. When the constraint $\bar{P}_{h,t}$ is high enough, for the *RA* scenario, our approach can fully satisfy the power demand when the number of PEV requesters is 20 at node 4. For the *free traveling* case, our approach can serve more PEVs since PEVs at node 4 can travel to node 1 and 3 directly without range anxiety limitations, while for *RA* case, the maximum number of PEVs flowing into node 1 and 3 is 10 due to the transporting range limitation. When the constraint $\bar{P}_{h,t}$ is decreased, fewer PEVs can be charged for all EVCS, especially for the *free traveling* case. At that time, the power allocation upper bound is the primary constraint to limit the PEV scheduling rather than the traveling range limitation. However, the proposed scheme still improves
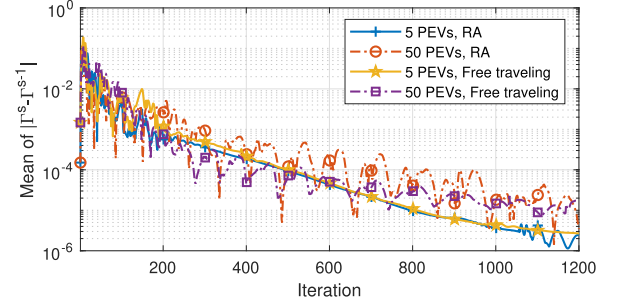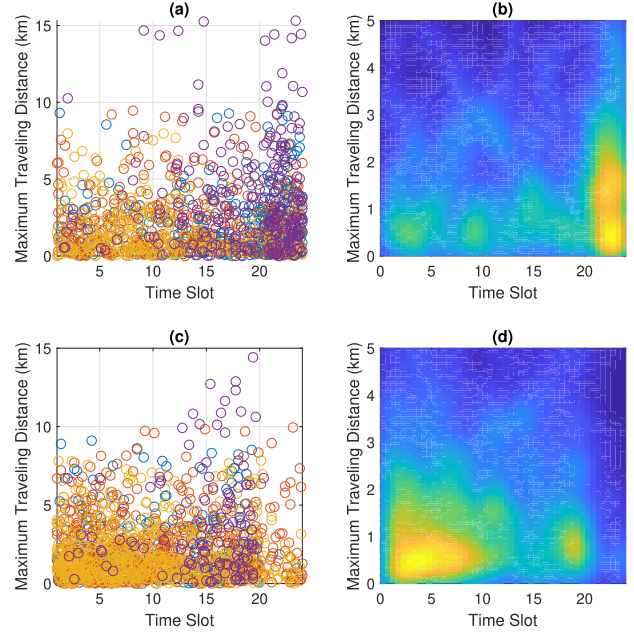
the charging capacity significantly compared with the greedy case. Moreover, the convergence performance of Algorithm 1 is shown in Fig. 5. When the iteration number around 800, for all cases, the value of stop criterion is under 10^{-4}.

C. Parameter Estimation for the Ten-Node Network

The transportation parameters are obtained by the data gathered from VISSIM. The historical profile of PEV maximum traveling range and the corresponding estimated distribution are shown in Fig. 6. The profile of PEVs arriving in four days is collected by EVCSs individually. The profiles of PEV requesters arriving EVCS 1 and 5 are shown in figures 6(a) and 6(c), respectively. The corresponding distribution estimation results, generated by kernel density estimation technique, are shown in figures 6(b) and 6(d). Since EVCS 1 is close to the Type 3 vehicle input point, the vehicles with high maximum traveling range, such as electric trucks, would have higher likeliness to enter EVCS 1 compared with EVCS 5, which is also reflected in the estimated distribution profile. In the estimated distribution, PEV requesters in
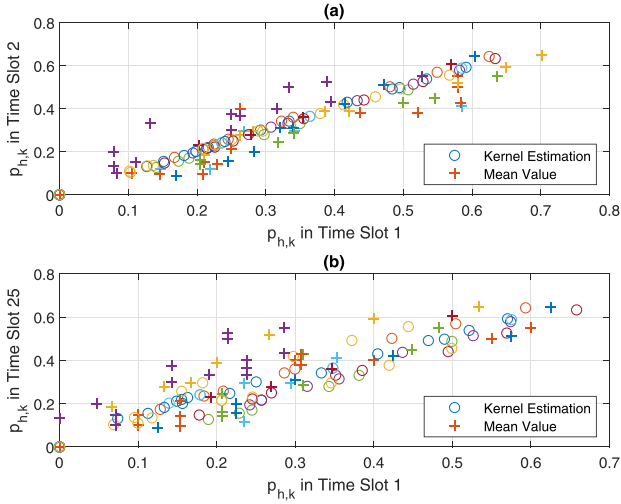
Fig. 7. (a) The correlation between the probability result $\{p_{h,k,t}, \forall h, k\}$ in slot 1 and 2. (b) The correlation between the probability result $\{p_{h,k,t}, \forall h, k\}$ in slot 1 and 25.
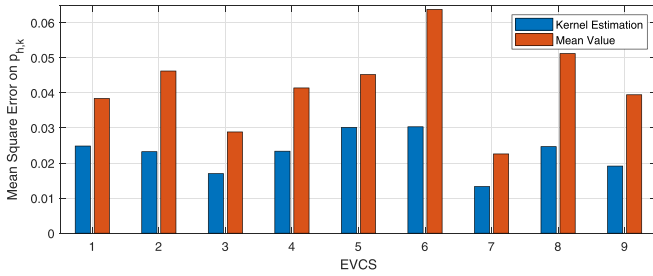

Fig. 8. Estimation error between kernel estimation method and the mean value methods.

EVCS 1 have a higher probability having long maximum traveling distance than PEV requesters in EVCS 5, especially at night.

The parameter estimation performance is shown in figures 7 and 8. We compare the kernel density estimation performance with the mean value method where the probability is obtained from the average number of PEVs, which can be shifted to another specific EVCS, divided by the overall PEV number. The scattered points in Fig. 7 represent the correlation of the estimated $\{p_{h,k,t}, \forall h, k \in \mathcal{G}\}$ in two time slots. As shown in Fig. 7(a), between the two consecutive slots, in which PEV's charging profile should be similar, the estimated probability between two slots are inclined to be identical, i.e., $p_{h,k,1} = p_{h,k,2}$, by our estimation method. However, the mean value method has higher variance on estimation between two consecutive slots. The correlation of estimated probability in slot 1 and slot 25 is shown in Fig. 7(b). The probability correlation is decreased due to the far time distance. Moreover, we explore PEV profile for two more days and compare the estimation error between the estimated spatial shifting probability and the real probability obtained from the six days. The mean square error for all stations is shown in Fig. 8. The result from the kernel density estimation method shows the lower error compared with the mean value method in all EVCSs.
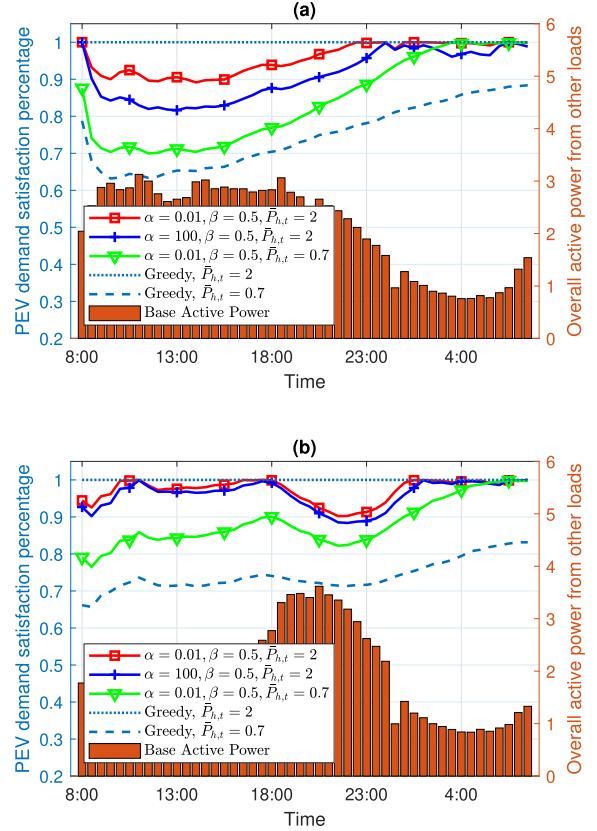

Fig. 9. Overall PEV demand satisfaction percentage with various penalty factor settings with (a) base load *pattern A*; (b) base load *pattern B*.

D. Power Allocation for the Ten-Node Network

The power allocation results for the ten-node network are provided in the subsection. We utilize the data set and PEV estimation results in Section VI-C. To reduce the simulation time, the subproblem (18) is calculated in a centralized manner.

The overall PEV demand satisfaction percentage among time slots is shown in Fig. 9, in which the bar graph represents the active power excluding PEV loads, i.e., base active power, in the distribution system. Our approach allocates less PEV power to avoid system overloading when the base active power is high and defers the PEV unscheduled demand to non-peak hours. With a lower spatial scheduling penalty α, the satisfaction percentage is increased since more PEV power is allocated to nodes near PCC for reducing voltage drop on the transmission line. Similarly, a high power allocation upper bound for a node in a time slot, i.e., a high $\bar{P}_{h,k}$ value, can also allow sufficient flexibility on PEV power allocation. Compared with greedy scheme, our proposed approach ensures that voltage drop is constrained. When the power allocation constraint is loose, i.e., $\bar{P}_{h,k} = 2$ p.u., although the greedy scheme can always satisfy the PEV power allocation, it cannot ensure voltage drop under the constraint, as shown in Fig. 10. Moreover, when the power allocation constraint is tight, i.e., $\bar{P}_{h,k} = 0.7$ p.u., by the end of the day, our proposed scheme still can ensure that all PEV demand is satisfied, i.e., the satisfaction percentage is one, while the greedy case cannot. PEV power allocation results for base load profile with
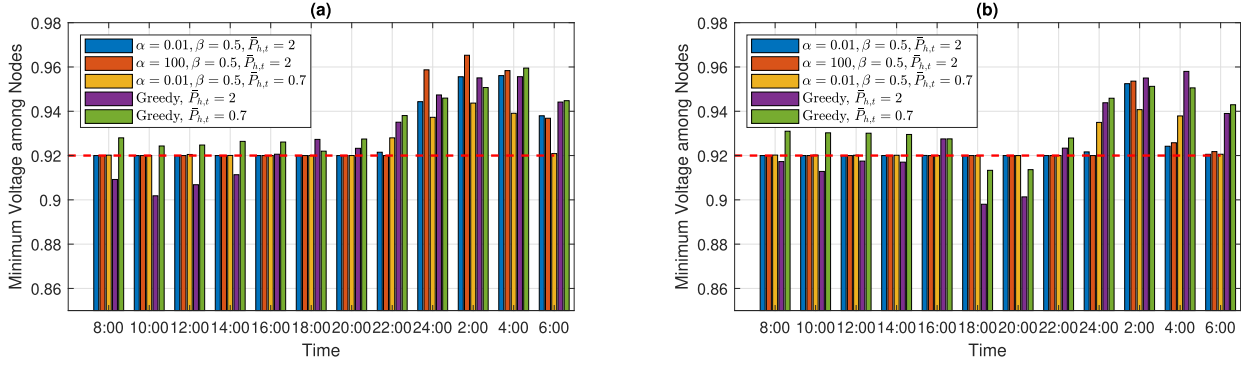
Fig. 10. The minimum voltage magnitude for the whole system in selected time slots with (a) base load *pattern A*; (b) base load *pattern B*.
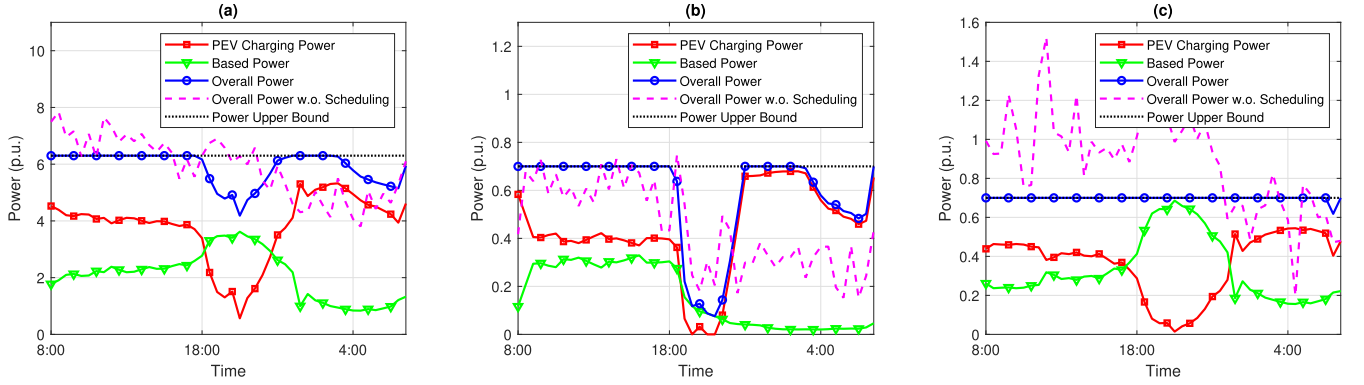

Fig. 11. The power profiles with and without scheduling (a) for the whole 10-node network; (b) for node 2; and (c) for node 4, where the base load follows *pattern B*, $\bar{P}_{h,t} = 0.7$ p.u., $\alpha = 0.01$, and $\beta = 0.5$.

pattern B are shown in Fig. 11. The overall power allocation for the whole network, node 2, and node 4 are shown in figures 11(a), 11(b), and 11(c), respectively. As shown in Fig. 11(a), our proposed approach schedules the PEV energy to fill the power valley in non-peak hours and shave the power peak in peak hours by temporal shifting, such that the overall power load can be balanced to avoid overloading. As shown in Fig. 10(b), from 18:00 to 20:00, if all PEV power is allocated as much as possible based on the upper bound of power allocation in charging stations, *i.e.*, greedy scheme, the voltage drop requirement cannot be guaranteed. To maintain voltage drop above the lower bound, our approach allocates less PEV power at that voltage-drop-violated period instead of allocating PEV power to fill the upper bound greedily. Furthermore, as shown in Fig. 11(c), PEV charging demand is too high to be fully accommodated by node 4; thus, a part of PEV demand needs to be shifted out, which can be observed from the gap between overall power allocation with and without scheduling. By contrast, as shown in Fig. 11(b), node 2 has relatively low PEV demand; thus, the node accepts the PEVs shifted from other nodes to increase the charging capacity for the whole system. It can be observed from the increased allocated energy in the node after scheduling. Note that all PEV demand can be fully scheduled and satisfied by the end of the day by our approach, as shown in Fig. 9(b). Compared with the case without scheduling, by spatio-temporal scheduling, we maximize the PEV energy allocated in the system without overloading the grid. The voltage drop requirement can also be guaranteed.

VII. CONCLUSION

In this paper, we have studied the problem of PEV charging power allocation among EVCSs. Based on constraints imposed by the existing power distribution system and the transportation network, the maximum service capacity for PEV charging has been achieved considering the power flow optimality and PEV range anxiety. A decentralized power allocation algorithm has been proposed to reduce time-complexity and communication overhead of power flow optimization for large-scale PEV charging. The proposed approach can be adopted by power utilities to coordinate a large number of PEVs charging in a power distribution system with multiple EVCSs. For the future work, the impact of PEV scheduling on the transportation system will be considered.

APPENDIX: DECOMPOSITION PROCESS OF (15)

The augmented Lagrange equation shown in (15) can be fully decomposed to $|\mathcal{G}|$ sub-equations except the following two terms with $\boldsymbol{\Delta}$:

$$u_{4,t}\bar{\Delta}_t + \rho_R \mathbf{u}_{8,t}^T(\mathbf{C}\boldsymbol{\Delta}_t - \mathbf{z}_{8,t}), \qquad (26)$$

and quadratic terms are ignored. To decompose the first term of (26), each node can calculate its own local variable,

$\Delta_{h,t}$, with the condition that $\Delta_{h,t}$ is in set $\mathcal{C}_1$ and $\mathcal{C}_2$, where

$$\mathcal{C}_1 = \{\Delta_{h,t}|\Delta_{1,t} + \cdots + \Delta_{|\mathcal{G}|,t} = 0\}, \tag{27a}$$

$$\mathcal{C}_2 = \{\Delta_{h,t}|\mathbf{C}(:,1)\Delta_{1,t} + \cdots + \mathbf{C}(:,|\mathcal{G}|)\Delta_{|\mathcal{G}|,t} \geq \mathbf{T}_t\}. \tag{27b}$$

Thus, each node h has the following sub-equation:

$$u_{4,t}^{(s-1)}(\Delta_{h,t} - \Delta_{h,t}^{(s-1)} + \bar{\Delta}_t^{(s-1)}) + \rho_R(\mathbf{u}_{8,t}^{(s-1)})^T$$

$$\left\{\frac{\mathbf{C}\Delta_t^{(s-1)}}{|\mathcal{G}|} + \mathbf{C}(:,h)(\Delta_{h,t} - \Delta_{h,t}^{(s-1)}) - \frac{\mathbf{z}_{8,t}^{(s-1)}}{|\mathcal{G}|}\right\} \tag{28}$$

To validate the equivalence between (26) and (28), we sum all sub-equations (28) for all $|\mathcal{G}|$ terms as follows:

$$u_{4,t}^{(s-1)}\left(\sum_h \Delta_{h,t} - \sum_h \Delta_{h,t}^{(s-1)} + |\mathcal{G}|\bar{\Delta}_t^{(s-1)}\right) + \rho_R(\mathbf{u}_{8,t}^{(s-1)})^T$$

$$\left\{\mathbf{C}\Delta_t^{(s-1)} + \sum_h \mathbf{C}(:,h)(\Delta_t - \Delta_t^{(s-1)}) - \mathbf{z}_{8,t}^{(s-1)}\right\}$$

$$= u_{4,t}^{(s-1)}\bar{\Delta}_t + \rho_R(\mathbf{u}_{8,t}^{(s-1)})^T(\mathbf{C}\Delta_t - \mathbf{z}_{8,t}^{(s-1)}). \tag{29}$$

At this point, problem (11) is fully decomposable.

REFERENCES

[1] L. Cai, J. Pan, L. Zhao, and X. Shen, "Networked electric vehicles for green intelligent transportation," *IEEE Commun. Standards Mag.*, vol. 1, no. 2, pp. 77–83, Jul. 2017.

[2] *Global EV Outlook 2017*, Int. Energy Agency, Paris, France, 2016.

[3] R. Zhou, Z. Li, C. Wu, and M. Chen, "Demand response in smart grids: A randomized auction approach," *IEEE J. Sel. Areas Commun.*, vol. 33, no. 12, pp. 2540–2553, Dec. 2015.

[4] J. A. P. Lopes, F. J. Soares, and P. M. R. Almeida, "Identifying management procedures to deal with connection of electric vehicles in the grid," in *Proc. IEEE Bucharest PowerTech*, Jun. 2009, pp. 1–8.

[5] G. Lacey, G. Putrus, and E. Bentley, "Smart EV charging schedules: Supporting the grid and protecting battery life," *IET Elect. Syst. Transp.*, vol. 7, no. 1, pp. 84–91, Mar. 2017.

[6] G. A. Putrus, P. Suwanapingkarl, D. Johnston, E. C. Bentley, and M. Narayana, "Impact of electric vehicles on power distribution networks," in *Proc. IEEE Vehicle Power Propuls. Conf.*, Sep. 2009, pp. 827–831.

[7] H. Liang, Y. Liu, F. Li, and Y. Shen, "Dynamic economic/emission dispatch including PEVs for peak shaving and valley filling," *IEEE Trans. Ind. Electron.*, vol. 66, no. 4, pp. 2880–2890, Apr. 2019.

[8] J. S. Vardakas, N. Zorba, and C. V. Verikoukis, "A survey on demand response programs in smart grids: Pricing methods and optimization algorithms," *IEEE Commun. Surveys Tuts.*, vol. 17, no. 1, pp. 152–178, Mar. 2015.

[9] P. He, M. Li, L. Zhao, B. Venkatesh, and H. Li, "Water-filling exact solutions for load balancing of smart power grid systems," *IEEE Trans. Smart Grid*, vol. 9, no. 2, pp. 1397–1407, Mar. 2018.

[10] M. Li, P. He, and L. Zhao, "Dynamic load balancing applying water-filling approach in smart grid systems," *IEEE Internet Things J.*, vol. 4, no. 1, pp. 247–257, Feb. 2017.

[11] Y. Wang, S. Mao, and R. M. Nelms, "Distributed online algorithm for optimal real-time energy distribution in the smart grid," *IEEE Internet Things J.*, vol. 1, no. 1, pp. 70–80, Feb. 2014.

[12] Y. Liu, R. Deng, and H. Liang, "A stochastic game approach for PEV charging station operation in smart grid," *IEEE Trans. Ind. Informat.*, vol. 14, no. 3, pp. 969–979, Mar. 2018.

[13] J. Li, C. Li, Y. Xu, Z. Y. Dong, K. P. Wong, and T. Huang, "Noncooperative game-based distributed charging control for plug-in electric vehicles in distribution networks," *IEEE Trans. Ind. Informat.*, vol. 14, no. 1, pp. 301–310, Jan. 2018.

[14] Z. Tan, P. Yang, and A. Nehorai, "An optimal and distributed demand response strategy with electric vehicles in the smart grid," *IEEE Trans. Smart Grid*, vol. 5, no. 2, pp. 861–869, Mar. 2014.

[15] L. Gan, U. Topcu, and S. H. Low, "Optimal decentralized protocol for electric vehicle charging," *IEEE Trans. Power Syst.*, vol. 28, no. 2, pp. 940–951, May 2013.

[16] M. Wang, H. Liang, R. Zhang, R. Deng, and X. Shen, "Mobility-aware coordinated charging for electric vehicles in VANET-enhanced smart grid," *IEEE J. Sel. Areas Commun.*, vol. 32, no. 7, pp. 1344–1360, Jul. 2014.

[17] R. Yu, W. Zhong, S. Xie, C. Yuen, S. Gjessing, and Y. Zhang, "Balancing power demand through EV mobility in vehicle-to-grid mobile energy networks," *IEEE Trans. Ind. Informat.*, vol. 12, no. 1, pp. 79–90, Feb. 2016.

[18] M. Zeng, S. Leng, Y. Zhang, and J. He, "QoE-aware power management in vehicle-to-grid networks: A matching-theoretic approach," *IEEE Trans. Smart Grid*, vol. 9, no. 4, pp. 2468–2477, Jul. 2018.

[19] J. Tan and L. Wang, "Real-time charging navigation of electric vehicles to fast charging stations: A hierarchical game approach," *IEEE Trans. Smart Grid*, vol. 8, no. 2, pp. 846–856, Mar. 2017.

[20] B. Zheng, P. He, L. Zhao, and H. Li, "A hybrid machine learning model for range estimation of electric vehicles," in *Proc. IEEE Global Commun. Conf. (GLOBECOM)*, Dec. 2016, pp. 1–6.

[21] W. Yuan, J. Huang, and Y. J. A. Zhang, "Competitive charging station pricing for plug-in electric vehicles," *IEEE Trans. Smart Grid*, vol. 8, no. 2, pp. 627–639, Mar. 2017.

[22] *VISSIM*. Accessed: Nov. 11, 2019. [Online]. Available: http://vision-traffic.ptvgroup.com/

[23] S. M. S. Hussain, T. S. Ustun, P. Nsonga, and I. Ali, "IEEE 1609 WAVE and IEC 61850 standard communication based integrated EV charging management in smart grids," *IEEE Trans. Veh. Technol.*, vol. 67, no. 8, pp. 7690–7697, Aug. 2018.

[24] S. Al-Rubaye, A. Al-Dulaimi, and Q. Ni, "Power interchange analysis for reliable vehicle-to-grid connectivity," *IEEE Commun. Mag.*, vol. 57, no. 8, pp. 105–111, Aug. 2019.

[25] P. Y. Kong and G. K. Karagiannidis, "Charging schemes for plug-in hybrid electric vehicles in smart grid: A survey," *IEEE Access*, vol. 4, pp. 6846–6875, Nov. 2016.

[26] E. Dall'Anese, H. Zhu, and G. B. Giannakis, "Distributed optimal power flow for smart microgrids," *IEEE Trans. Smart Grid*, vol. 4, no. 3, pp. 1464–1475, Sep. 2013.

[27] R. A. Jabr, "Exploiting sparsity in SDP relaxations of the OPF problem," *IEEE Trans. Power Syst.*, vol. 27, no. 2, pp. 1138–1139, May 2012.

[28] R. Baldick, B. H. Kim, C. Chase, and Y. Luo, "A fast distributed implementation of optimal power flow," *IEEE Trans. Power Syst.*, vol. 14, no. 3, pp. 858–864, Aug. 1999.

[29] S. Bose, D. F. Gayme, S. Low, and K. M. Chandy, "Optimal power flow over tree networks," in *Proc. 49th Annu. Allerton Conf. Commun., Control, Comput. (Allerton)*, Sep. 2011, pp. 1342–1348.

[30] J. Lavaei and S. H. Low, "Zero duality gap in optimal power flow problem," *IEEE Trans. Power Syst.*, vol. 27, no. 1, pp. 92–107, Feb. 2012.

[31] Z.-Q. Luo, W.-K. Ma, A. M.-C. So, Y. Ye, and S. Zhang, "Semidefinite relaxation of quadratic optimization problems," *IEEE Signal Process. Mag.*, vol. 27, no. 3, pp. 20–34, May 2010.

[32] B. Zhang, A. Y. S. Lam, A. D. Domínguez-García, and D. Tse, "An optimal and distributed method for voltage regulation in power distribution systems," *IEEE Trans. Power Syst.*, vol. 30, no. 4, pp. 1714–1726, Jul. 2015.

[33] W. Deng, M.-J. Lai, Z. Peng, and W. Yin, "Parallel multi-block ADMM with o(1/k) convergence," *J. Sci. Comput.*, vol. 71, pp. 712–736, May 2017.

[34] A. Sootla, "Model reduction using semidefinite programming," Licentiate thesis, Dept. Autom. Control, Lund Univ., Lund, Sweden, Nov. 2009. Accessed: Nov. 11, 2019. [Online]. Available: http://www.control.lth.se/publications/

[35] I. S. Bayram, G. Michailidis, M. Devetsikiotis, and F. Granelli, "Electric power allocation in a network of fast charging stations," *IEEE J. Sel. Areas Commun.*, vol. 31, no. 7, pp. 1235–1246, Jul. 2013.

[36] O. Hafez and K. Bhattacharya, "Queuing analysis based PEV load modeling considering battery charging behavior and their impact on distribution system operation," *IEEE Trans. Smart Grid*, vol. 9, no. 1, pp. 261–273, Jan. 2018.

[37] R. Cao, A. Cuevas, and W. G. Manteiga, "A comparative study of several smoothing methods in density estimation," *Comput. Statist. Data Anal.*, vol. 17, no. 2, pp. 153–176, Feb. 1994.

[38] J. A. Jardini, C. M. V. Tahan, M. R. Gouvea, S. U. Ahn, and F. M. Figueiredo, "Daily load profiles for residential, commercial and industrial low voltage consumers," *IEEE Trans. Power Del.*, vol. 15, no. 1, pp. 375–380, Jan. 2000.
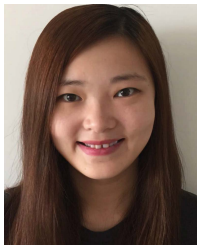
Mushu Li received the B.Eng. degree from the University of Ontario Institute of Technology (UOIT), Oshawa, Canada, in 2015, and the M.A.Sc. degree from Ryerson University, Toronto, Canada, in 2017. She is currently pursuing the Ph.D. degree in electrical engineering with the University of Waterloo, Canada. Her research interests include the system optimization in VANETs and PEV charging scheduling. She was a recipient of the NSERC CGS Scholarship in 2018, and OGS in 2015 and 2016.
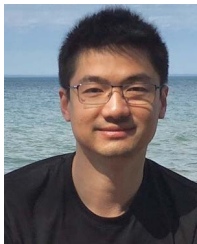
Jie Gao (S'09–M'17) received the B.Eng. degree in electronics and information engineering from the Huazhong University of Science and Technology, Wuhan, China, in 2007, and the M.Sc. and Ph.D. degrees in electrical engineering from the University of Alberta, Edmonton, AB, Canada, in 2009 and 2014, respectively. He is currently a Research Associate with the Department of Electrical and Computer Engineering, University of Waterloo. His research interests include the application of game theory, mechanism design, and optimization methods for distributed decision making and network utility maximization in wireless communication networks. He was a recipient of the Alberta Innovates-Technology Futures Scholarship, the Ontario Centres of Excellence TalentEdge Fellowship, and the Natural Science and Engineering Research Council of Canada Postdoctoral Fellowship.

Nan Chen received the B.S. degree in electrical engineering from the Nanjing University of Aeronautics and Astronautics, Nanjing, Jiangsu, China, in 2014, and the Ph.D. degree in electrical and computer engineering from the University of Waterloo, Waterloo, ON, Canada, in 2019. She is currently a Post-Doctoral Fellow with the Department of Electrical and Computer Engineering, University of Waterloo. Her current research interests include electric vehicle charging/discharging strategy in smart grid and artificial intelligence-enabled next-generation networks.

Lian Zhao (S'99–M'03–SM'06) received the Ph.D. degree from the Department of Electrical and Computer Engineering (ELCE), University of Waterloo, ON, Canada, in 2002.

She joined the Department of Electrical and Computer Engineering, Ryerson University, Toronto, Canada, in 2003, where she became a Professor in 2014. Her research interests include wireless communications, resource management, mobile edge computing, communication and caching, network slicing, and scalable network control. She is a Senior Member of the IEEE Communication and Vehicular Society. She served as a Committee Member of the Natural Science and Engineering Research Council of Canada (NSERC) Discovery Grants Evaluation Group for Electrical and Computer Engineering from 2015 to 2018. She received the Best Land Transportation Paper Award from the IEEE Vehicular Technology Society in 2016, the Top 15 Editor Award in 2015 for the IEEE TRANSACTIONS ON VEHICULAR TECHNOLOGY, the Best Paper Award from the 2013 International Conference on Wireless Communications and Signal Processing (WCSP), the Best Student Paper Award (with her student) from Chinacom in 2011, the Canada Foundation for Innovation (CFI) New Opportunity Research Award in 2005, and an Early Tenure and promotion to Associate Professor in 2006. She serves as the General Co-Chair for the IEEE GreeenCom 2018, the Co-Chair for the IEEE ICC 2018 Wireless Communication Symposium, the Workshop Co-Chair for the IEEE/CIC ICCC 2015, and the Co-Chair for the IEEE Global Communications Conference (GLOBECOM) 2013 Communication Theory Symposium. She serves on the Editorial Board for the IEEE TRANSACTIONS ON VEHICULAR TECHNOLOGY, the IEEE INTERNET OF THINGS JOURNAL, and the *Transactions on Emerging Telecommunication Technologies*. She is a licensed Professional Engineer in the Province of Ontario.

Xuemin (Sherman) Shen (M'97–SM'02–F'09) received the B.Sc. degree from Dalian Maritime University, Dalian, China, in 1982, and the M.Sc. and Ph.D. degrees from Rutgers University, New Brunswick, NJ, USA, in 1987 and 1990, respectively, all in electrical engineering.

He is currently a University Professor and an Associate Chair for Graduate Studies with the Department of Electrical and Computer Engineering, University of Waterloo, ON, Canada. His research focuses on resource management, wireless network security, social networks, smart grid, and vehicular ad hoc and sensor networks. He is a registered Professional Engineer of ON, Canada, an Engineering Institute of Canada Fellow, a Canadian Academy of Engineering Fellow, and a Royal Society of Canada Fellow. He was a recipient of the Outstanding Performance Award five times from the University of Waterloo, the Premier's Research Excellence Award (PREA) in 2003 from the Province of Ontario, Canada, the Excellent Graduate Supervision Award in 2006, the Joseph LoCicero Award in 2015, the Education Award in 2017 from the IEEE Communications Society, the James Evans Avant Garde Award in 2018 from the IEEE Vehicular Technology Society, and the R. A. Fessenden Award in 2019 from IEEE, Canada. He is a Distinguished Lecturer of the IEEE Vehicular Technology Society and the Communications Society. He served as the Technical Program Committee Chair/Co-Chair for the IEEE Globecom'16, the IEEE Infocom'14, the IEEE Vehicular Technology Conference'10 Fall, and the IEEE Globecom'07, the Symposia Chair for the IEEE International Conference on Communications'10, the Tutorial Chair for the IEEE Vehicular Technology Conference'11 Spring, and the Chair for the IEEE Communications Society Technical Committee on Wireless Communications, and P2P Communications and Networking. He is the Editor-in-Chief of the IEEE INTERNET OF THINGS JOURNAL and the Vice President of Publications of the IEEE Communications Society.